Received: 12 September 2020 | Revised: 20 October 2020 | Accepted: 5 November 2020

DOI: 10.1002/num.22670

RESEARCH ARTICLE

WILEY

Hall and ion slip effects on magnetohydrodynamic convective rotating flow of Jeffreys fluid over an impulsively moving vertical plate embedded in a saturated porous medium with Ramped wall temperature

M. Veera Krishna[1] | **Ali J. Chamkha**[2,3]

[1]Department of Mathematics, Rayalaseema University, Kurnool, India
[2]Institute of Research and Development, Duy Tan University, Da Nang, Vietnam
[3]Institute of Theoretical and Applied Research (ITAR), Duy Tan University, Hanoi, Vietnam

Correspondence
M. Veera Krishna, Department of Mathematics, Rayalaseema University, Kurnool, Andhra Pradesh 518007, India.
Email: veerakrishna_maths@yahoo.com

Abstract

In the present study, it is explored theoretically Hall and ion slip effects on the unsteady magnetohydrodynamic (MHD) rotating flow of a viscous, incompressible electrically conducting, and optically thick radiating Jeffreys fluid over an impulsively, moving vertical plate embedded in a saturated porous medium, when the temperature of the plate has a provisionally ramped profile. The exact solutions of the governing equations for the flow domain are attained by making use of the Laplace transform method. The specified analytical solutions are also acquired for some limiting cases. The research phrases of engineering curiosity for skin friction and Nusselt number are originated for both ramped wall temperature and the isothermal plate. Sherwood number is also obtained. The numerical results of velocity, temperature, and concentration distributions are exhibited graphically whereas skin friction, Nusselt number, and also Sherwood number are mentioned in a table form. It is observed that on either cases of ramped wall temperature and isothermal plate, the resultant velocity enhances with an increase in Hall and ion slip parameters. Reversal behavior is observed with an increase in magnetic field parameter, Jeffreys fluid parameter and Prandtl number. Thermal and concentration buoyancy forces and thermal radiation tend to accelerate the resultant velocity throughout the boundary layer region. The temperature reduces with an increase in Prandtl number and reverse

effect is observed with an increase in thermal radiation parameter. Mass diffusion tends to enhance to species concentration. The rotation and Jeffreys fluid parameters tend to enhance both stress components. Nusselt number enables to lessen with growing in thermal radiation parameter and is magnified on escalating in time. The Sherwood number is improved with increasing in Schmidt number at the plate and it is refused on increasing in time.

KEYWORDS

convection flows, Hall and ion-slip effects, MHD flows, porous medium, ramped temperature

1 | INTRODUCTION

The flow through porous media has a number of applications in physiological and engineering streams. Efforts in these applications include food movement from the digestive tract, urine transmission from the kidney to the bladder, sperm motility and male reproductive tract, the uterine canal, ovarian transportation of the females fallopian tubes, vasomotions of little blood vessels, hygienic liquid transportation, roller, as well as finger pumps, hosepipes, toxic fluid transport and corrosive fluid transport in nuclear engineering and manufacturing etc. Such as dialysis machines, pumping blood to the lungs by the heart, biomedical devices, and engineers are going through this process. The aforementioned applications are plentiful in the novel of peristalsis. It is established as heat transport to perform an imperative task in attractive fact on the physical property of living tissue. Heat transport is essential where the thermodynamic differences are important in oxygenation and hepatitis, cancer, and blood pressure. The combined effects are attained for heat and heavy water transport on chemicals, food, paper, and machine building efforts. Natural convection flow induced by thermal and solutal buoyancy forces acting over bodies with different geometries in a fluid saturated porous medium is prevalent in many natural phenomena and has varied and wide range of industrial applications. For example, in atmospheric flows, the presence of pure air or water is impossible because some foreign mass may be present either naturally or mixed with air or water due to industrial emissions. Natural processes such as attenuation of toxic waste in water bodies, vaporization of mist and fog, photosynthesis, drying of porous solids, transpiration, sea-wind formation (where upward convection is modified by Coriolis forces), and formation of ocean currents occur due to thermal and solutal buoyancy forces developed as a result of difference in temperature or concentration or a combination of these two. Such configuration is also encountered in several practical systems for industry based applications viz. heat exchanger devices, cooling of molten metals, insulation systems, petroleum reservoirs, filtration, chemical catalytic reactors and processes, nuclear waste repositories, desert coolers, wet bulb thermometers, frost formation in vertical channels, and so on.

In view of the significance by the fluid flow problems, extensive and deepness of research works have been made by several investigators. Awaludin et al. [1] explored the stability investigation of stagnation indicates flow movement over an extending or contracting sheet. Bejan and Khair [2] discussed the heat and mass transport through the natural convective flow movement in a porous medium. Radiation and mass transport effects on free convection flow movement over a semi-infinite vertical plate have been examined by Chamkha et al. [3]. Eckert and Drake [4] discussed a clear analysis of

heat and mass transport through various channels or conduits. Ganesan and Palani [5] explored the natural convective flows on an impulsively initiated and inclined surface by means of heat and mass transport. Gebhart et al. [6] have discussed the buoyancy induced flow of viscous incompressible fluids and heat transfer. Jang and Chang [7] investigated buoyancy induced and inclined boundary layer flow in a porous medium effecting from combined heat and mass buoyancy forces. The non-Darcian free and forced convective flow movement over a vertical wall in a soaked porous medium has been addressed by Lai and Kulacki [8]. Nakayama and Hossain [9] explored the integral behavior for both heat and mass transfer through free convection flow in a permeable medium. Nield and Bejan [10] discussed free and forced convective flows in porous medium in various configurations. Pop and Ingham [11] explored the mathematical and computational modeling for the convective heat transfer of viscous incompressible fluids through porous media. Raptis [12] discussed the natural convective and mass transfer effects for the oscillating flow movement over an infinite moving vertical isothermal surface with invariable suction and heat sources. The numerous solutions of MHD boundary layer flow and heat transfer performance of nanofluids through a power-law extending or contracting porous sheet by an effect of viscous dissipation has been explored by Ruchika et al. [13].

It is noticed that when the density of an electrically conducting fluid is low and/or applied magnetic field is strong, Hall current is produced in the flow-field which plays an important role in determining flow features of the problems because it induces secondary flow in the flow-field. Keeping in view this fact, significant investigations on MHD free convection flow past a flat plate with Hall effects under different thermal conditions are carried out by several researchers in the past. Investigation of MHD natural convection flow in a rotating medium is of considerable importance due to its application in various areas of geophysics, astrophysics and fluid engineering viz. maintenance and secular variations in Earth's magnetic field due to motion of Earth's liquid core, internal rotation rate of the Sun, structure of the magnetic stars, solar and planetary dynamo problems, turbo machines, rotating MHD generators, rotating drum separators for liquid metal MHD applications, etc. It may be noted that Coriolis and magnetic forces are comparable in magnitude and Coriolis force induces secondary flow in the flow-field. Taking into consideration the importance of such study, unsteady MHD natural convection flow past a moving plate in a rotating medium is studied by a number of researchers. Recently, Krishna and Chamkha [14] investigated the Hall and ion slip effects on the MHD convective flow of elastico-viscous fluid through porous medium between two rigidly rotating parallel plates with time fluctuating sinusoidal pressure gradient. The combined effects of Hall and ion slip on MHD rotating flow of ciliary propulsion of microscopic organism through porous medium have been studied by Krishna et al. [15]. Abd El-Aziz [16] investigated the dual solutions of MHD stagnation point flow and heat transfer towards a stretching/shrinking sheet with nonuniform heat source/sink and variable surface heat flux. Shahazad et al. [17] discussed on unsteady axi-symmetric flow and heat transport over time dependent radially stretching sheet. Turkyilmazoglu [18] reported the heat transfer on MHD flow of a micro-polar fluid due to an infinite stretching porous surface. Baag et al. [19] discussed entropy generation analysis for MHD flow of visco-elastic fluid past a stretching sheet embedded in an absorbent surface. Ahmed et al. [20] examined the convective boundary conditions on MHD axi-symmetric flow of power-law fluid over an unsteady stretching sheet. Fauzi et al. [21] discussed heat transfer on stagnation point flow over a nonlinear shrinking sheet with slip effect. Hakeem et al. [22] investigated second order MHD slip flow of Nanofluid through a porous surface. Bhattacharyya and Pop [23] examined the MHD boundary layer flow movement due to an exponentially shrinking sheet. Bhattacharyya [24] explored the effects of radiation and heat source or sink on unsteady MHD boundary layer flow of the viscous fluid over a shrinking sheet with heat transfer and suction or injection. The effects of heat source or sink on MHD flow of the viscous fluid past a shrinking sheet with heat transport and mass suction has been investigated by Bhattacharyya [25]. Imtiaz et al.

[26] discussed for the MHD flow of Jeffreys fluid by means of the curved stretching surface with homogeneous–heterogeneous reactions. Sandeep and Sulochana [27] are carried out research on the heat transport of non-Newtonian nanofluids through a stretching surface along with nonhomogeneous heat source or sink. Ahmad et al. [28] researched the combined convective flow past an exponentially stretching sheet. MHD stagnation point flow of Jeffreys fluid by a radially stretching surface with viscous dissipation and Joule heating has been discussed by Hayat et al. [29]. Kalidas et al. [30] researched the radiative flow of MHD Jeffreys fluid past a stretching sheet with surface slip and melting heat transfer. The effects of radiation and Hall currents for an unsteady MHD free convection flow during a vertical conduit packed by means of a porous medium has been explored by Krishna et al. [31]. The heat generation or absorption and thermo-diffusion for an unsteady free convection MHD flow of radiating and chemically reacting second grade fluid past an infinite vertical surface during a permeable medium and adopting the Hall currents into description has been researched by Krishna and Chamkha [32]. Hall and ion slip effects on the unsteady MHD convective rotating flow of nanofluids with applications in biomedical engineering has been explored by Krishna and Chamkha [33]. Krishna et al. [34] discussed the Hall and ion slip effects for the unsteady MHD free convective rotating flow through porous medium over an exponential accelerated plate. Krishna et al. [35] explored the Hall effects on the MHD peristaltic flow of Jeffreys fluid through porous medium in a vertical stratum.

Heat transfer, free convective flow and entropy generation of water, Al_2O_3–water, and nano-encapsulated phase change material diluted in water as nano-encapsulated phase change material-water suspension in a hot enclosure has been studied by Hashemi-Tilehnoee et al. [36]. Sadeghi et al. [37] examined the magnetic natural convection within a novel nanoliquid filled-enclosure with wavy wall and trapezoidal heater considering interior heat generation using finite element method. Mondal et al. [38] discussed the natural convection nanofluid flow in an annulus between a circular cylinder and a rhombus enclosure. Dogonchi et al. [39] described the importance of the Cattaneo–Christov theory of heat conduction in a triangular enclosure with a semi-circular heater subjected to Fe_3O_4–H_2O nanofluid, heat generation and shape factor of nanoparticles and viscosity dependent on magnetic field is taken into consideration to simulate ferrofluid viscosity. Hashemi-Tilehnoee et al. [40] studied entropy generation analysis in the concentric annuli of a gas insulation transmission line enclosure loaded with air and SF_6–N_2 mixture gas. Singh et al. [41] presented for the MHD convective flow of visco-elastic fluid through a vertical channel bounded by the porous regime with Hall current and induced magnetic field effects. The MHD free convective flow of visco-elastic fluid through a porous regime in an inclined channel taking the Hall and ion-slip effects has been investigated by Singh and Vishwanath [42]. Singh et al. [43] investigated the steady MHD mixed convection flow of a visco-elastic fluid over a magnetized vertical surface embedded in a uniform porous material with rotation, the Hall and induced magnetic field effects using the regular perturbation technique. The MHD boundary layer flow of Walters'-B fluid over a vertical porous surface implanted in a porous material under the action of a strong external applied magnetic field and rotation has been presented by Singh et al. [44]. The unsteady MHD boundary layer flow of a rotating Walters'-B fluid over an infinite vertical porous plate embedded in a uniform porous medium with fluctuating wall temperature and concentration taking Hall and ion-slip effects into consideration is discussed by Singh et al. [45]. Singh et al. [46] explored the analytical solutions on an unsteady MHD boundary layer flow of a rotating visco-elastic fluid over an infinite vertical porous plate embedded in a uniform porous medium with oscillating free-stream taking Hall and ion-slip currents into account. The steady MHD mixed convective generalized Couette flow between two infinite parallel plates filled with a porous medium in a rotating system with the Hall effects has been presented by Singh et al. [47]. Seth and Singh [48] explored the mixed convection MHD flow of a viscous, incompressible, electrically and thermally conducting fluid in a rotating channel taking Hall current into account. The entropy

generation, fluid flow, and heat transfer regarding Cu–Al_2O_3–water hybrid nanofluids into a complex shape enclosure containing a hot-half partition have been addressed by Alsabery et al. [49]. The thermal and hydrodynamic characteristics of a suspension with water-nano-encapsulated phase change material in an annulus of a porous eccentric horizontal cylinder have been investigated by Ghalambaz et al. [50]. Zadeh et al. [51] discussed the numerical analysis of entropy generation in the natural convection of water combined with nano-sized particles containing the encapsulated phase change material in a square enclosure with a solid triangular block with the finite element method. The free convective flow of a nano-encapsulated phase change material suspension in an eccentric annulus has been investigated numerically by Mehryan et al. [52]. Ghalambaz et al. [53] investigated melting flow and heat transfer of electrically conductive phase change materials subjecting to a nonuniform magnetic field in a square enclosure. Mehryan et al. [54] discussed an effective heat transfer agent or by increasing the heat transfer surface to use the phase change material with nanoparticles for an intensification of heat removal within a gap between two coaxial vertical isothermal cylinders and was performed numerically using the Galerkin finite element approach. Krishna [55] investigated the influence of thermal radiation, Hall and ion-slip impacts on the unsteady MHD free convective rotating flow of Jeffreys fluid past an infinite vertical porous plate with the ramped wall temperature.

Keeping the above mentioned information, the Hall and ion slip effects on the unsteady MHD rotating flow of a viscous optically thick radiating Jeffreys fluid over an impulsively moving vertical plate in a saturated porous medium, the temperature of the plate has a provisionally ramped profile has not been established yet. Therefore, in this paper, it is addressed Hall and ion slip effects on the unsteady MHD rotating flow of a viscous, incompressible electrically conducting, and optically thick radiating Jeffreys fluid over an impulsively, moving vertical plate embedded in a saturated porous medium, when the temperature of the plate has a provisionally ramped profile. This investigation organized in five sections. Section 2 contains problem statement, its modeling and solution procedure is given. Results and discussion are described in detail in Section 3. It is also discussed code validation in Section 4. Finally the conclusions are specified in Section 5.

2 | FORMULATION AND SOLUTION OF THE PROBLEM

We assumed the unsteady MHD rotating flow of a viscous, incompressible electrically conducting, and optically thick radiating Jeffreys fluid over an impulsively, moving vertical plate embedded in a saturated porous medium, when the temperature of the plate has a provisionally ramped profile and taking Hall and ion slip impacts into account described by the following equations.

$$\nabla.\mathbf{V} = 0, \tag{1}$$

$$\rho\left(\frac{\partial \mathbf{V}}{\partial t} + (\mathbf{V}\cdot\nabla)\mathbf{V} + 2\Omega\times\mathbf{V} + \Omega\times(\Omega\times\mathbf{r})\right) = \operatorname{div}\mathbf{T} + \mathbf{J}\times\mathbf{B} + \mathbf{R}, \tag{2}$$

$$\nabla\times\mathbf{E} = -\frac{\partial \mathbf{B}}{\partial t}, \nabla\times\mathbf{B} = \mu_m\mathbf{J}, \operatorname{div}\mathbf{B} = \mathbf{0}, \tag{3}$$

where $\mathbf{V}$ is the velocity vector, T is the Cauchy stress tensor of Jeffreys fluid, ρ is the fluid density, $\mathbf{R}$ is Darcy's resistance and some physical variables appearing in Equations (1)–(3) through Maxwell's equations are $\mathbf{J}$, $\mathbf{B}$, $\mathbf{E}$, and μ_m are vector of current density, entire magnetic field, electric field, and magnetic permeability accordingly. The total strength of magnetic field is $\mathbf{B} = B_0 + b$, where B_0 is the strength of applied magnetic field vector and b is the induced magnetic field vector, and Ω is the angular velocity as well as $\mathbf{r}$ is radial co-ordinate specified through $r^2 = x^2 + y^2$.

The constitutive equations for Jeffreys fluids are,

$$\mathbf{T} = p\mathbf{I} + \mathbf{S}, \tag{4}$$

$$\mathbf{S} = \frac{\mu}{1+\lambda_1}\left(\mathbf{A}_1 + \lambda_2\left(\frac{\partial \mathbf{A}_1}{\partial t} + (\mathbf{V}\cdot\nabla)\mathbf{A}_1\right)\right), \tag{5}$$

where $p\mathbf{I}$ is the indeterminate part of stress tensor, $\mathbf{S}$ is the extra stress tensor, μ is the viscosity of the fluid, λ_1 and λ_2 are the relaxation and retardation times and $\mathbf{A}_1$ is the Rivlin–Erickson tensor defined as,

$$\mathbf{A}_1 = \nabla\mathbf{V} + (\nabla\mathbf{V})^T \tag{6}$$

The modified Darcy's law for the Jeffreys fluid is given by,

$$\mathbf{R} = -\frac{\mu\varphi}{K_1(1+\lambda_1)}\left(1 + \lambda_2\frac{\partial}{\partial t}\right)\mathbf{V}. \tag{7}$$

It is considered that the Cartesian co-ordinate system, the x-axis is the length of the plate in upward direction as well as the y-axis perpendicular to surface of the plate in the fluid region. A uniform transverse magnetic field B_0 is applied in a direction this is horizontal to y-axis. Both the fluid and plate rotate in unison through unvarying angular velocity Ω about the y-axis. The physical modeling of the problem is shown in Figure 1. Initially at the time $t \leq 0$, both the fluid and plate are at rest and are maintained at a uniform temperature T_∞. Also species concentration at the surface of the plate in addition at each point within the fluid and is maintained at uniform concentration C_∞. At the time $t > 0$, the plate is moving along the x-direction with uniform velocity U_0 in its own plane. The temperature of plate is expanded or depressed to $T_\infty + (T_w - T_\infty)(t/t_0)$ when $0 < t \leq t_0$, and it is maintained at the uniform temperature T_w after $t > t_0$ (t_0 being characteristic time). Also, at the time $t > 0$, species concentration at the surface of the plate is raised to uniform species concentration C_w and also it is maintained thereafter. In sight of the detailed that, the plate is of infinite extent in x and z directions and is electrically nonconducting, then all physical variables except pressure are depend on y and t alone. Also no applied or polarized voltages exist so the effect of polarization of fluid is negligible. This corresponds to the case where no energy is added or extracted from the fluid by electrical means. It is assumed that the induced magnetic field generated by fluid motion is negligible in comparison to the applied one. This assumption is justified because magnetic Reynolds number is very small for liquid metals and partially ionized fluids which are commonly used in industrial applications. Keeping in view the assumptions made above, governing equations for natural convection flow of an electrically conducting, viscous, incompressible and optically thick radiating Jeffreys fluid through a saturated porous medium in a rotating frame of reference taking Hall and ion slip effects into account. Under the assumptions of a small magnetic Reynolds number and under Boussinesq approximation the governing equations are obtained [56] as,

$$\frac{\partial u}{\partial t} + 2\Omega w = \frac{\nu}{1+\lambda_1}\left(1 + \lambda_2\frac{\partial}{\partial t}\right)\frac{\partial^2 u}{\partial y^2} - \frac{B_0 J_z}{\rho} - \frac{\nu\varphi}{k(1+\lambda_1)}\left(1 + \lambda_2\frac{\partial}{\partial t}\right)u + g\beta(T - T_\infty) + g\beta^*(C - C_\infty), \tag{8}$$

$$\frac{\partial w}{\partial t} - 2\Omega u = \frac{\nu}{1+\lambda_1}\left(1 + \lambda_2\frac{\partial}{\partial t}\right)\frac{\partial^2 w}{\partial y^2} + \frac{B_0 J_x}{\rho} - \frac{\nu\varphi}{k(1+\lambda_1)}\left(1 + \lambda_2\frac{\partial}{\partial t}\right)w. \tag{9}$$

The electron-atom collision frequency is assumed to be very high, so that Hall and ion slip currents cannot be neglected. Hence, the Hall and ion slip currents give rise to the velocity in z-direction. When the strength of the magnetic field is very large, the generalized Ohm's law is modified to incorporate

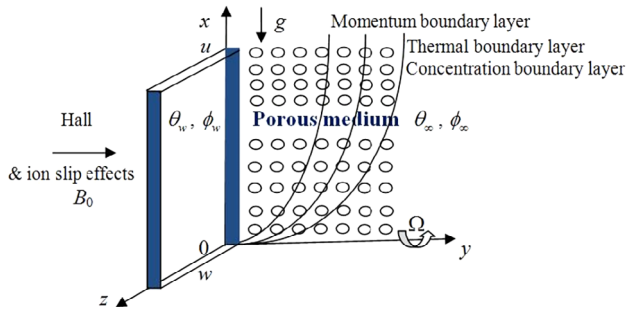

FIGURE 1 Physical model of the problem [Color figure can be viewed at wileyonlinelibrary.com]

the Hall and ion slip effects [57],

$$\mathbf{J} = \sigma\,(\mathbf{E} + \mathbf{V} \times \mathbf{B}) - \frac{\omega_e \tau_e}{B_0}\,(\mathbf{J} \times \mathbf{B}) + \frac{\omega_e \tau_e \beta_i}{B_0^2}\,((\mathbf{J} \times \mathbf{B}) \times \mathbf{B}). \tag{10}$$

Furthermore, it is assumed that the Hall parameter $\beta_e = \omega_e \tau_e \approx \mathrm{O}(1)$ as well as ion slip parameter $\beta_i = \omega_i \tau_i \ll 1$, in the Equation (10), the electron pressure gradient and thermo-electric effects are neglected, that is, $\mathbf{E} = (0, 0, 0)$, under these assumptions, the components forms of Equation (10) to be,

$$(1 + \beta_i \beta_e) J_x - \beta_e J_z = -\sigma B_0 w, \tag{11}$$

$$(1 + \beta_i \beta_e) J_z + \beta_e J_x = \sigma B_0 u. \tag{12}$$

On solving Equations (11) and (12), we acquired,

$$J_x = \sigma B_0 (\alpha_2 u - \alpha_1 w), \tag{13}$$

$$J_z = \sigma B_0 (\alpha_1 u + \alpha_2 w), \tag{14}$$

where $\alpha_1 = \frac{1+\beta_e\beta_i}{(1+\beta_e\beta_i)^2+\beta_e^2}$ and $\alpha_2 = \frac{\beta_e}{(1+\beta_e\beta_i)^2+\beta_e^2}$.

Substituting Equations (13) and (14) in (9) and (8) accordingly, it is obtained the equations of the flow through the reference to a rotating frame are specified to be

$$\frac{\partial u}{\partial t} + 2\Omega w = \frac{\nu}{1+\lambda_1}\left(1 + \lambda_2 \frac{\partial}{\partial t}\right)\frac{\partial^2 u}{\partial y^2} - \frac{\sigma B_0^2 (\alpha_1 u + \alpha_2 w)}{\rho} - \frac{\nu \varphi}{k(1+\lambda_1)}\left(1 + \lambda_2 \frac{\partial}{\partial t}\right) u + g\beta(T - T_\infty) + g\beta^*(C - C_\infty), \tag{15}$$

$$\frac{\partial w}{\partial t} - 2\Omega u = \frac{\nu}{1+\lambda_1}\left(1 + \lambda_2 \frac{\partial}{\partial t}\right)\frac{\partial^2 w}{\partial y^2} - \frac{\sigma B_0^2 (\alpha_1 w - \alpha_2 u)}{\rho} - \frac{\nu \varphi}{k(1+\lambda_1)}\left(1 + \lambda_2 \frac{\partial}{\partial t}\right) w, \tag{16}$$

$$\rho C_p \frac{\partial T}{\partial t} = k_1 \frac{\partial^2 T}{\partial y^2} - \frac{\partial q_r}{\partial y}, \tag{17}$$

$$\frac{\partial C}{\partial t} = D\,\frac{\partial^2 C}{\partial y^2}. \tag{18}$$

The initial and boundary conditions are,

$$u = w = 0, T = T_\infty, C = C_\infty \text{ for } y \geq 0 \text{ and } t \leq 0, \tag{19}$$

$$u = U_0, w = 0 \quad \text{at } y = 0 \text{ for } t > 0, \tag{20}$$

$$T = T_\infty + (T_w - T_\infty)(t/t_0) \text{ at } y = 0 \text{ for } 0 < t \le t_0, \tag{21}$$

$$T = T_w \quad \text{at } y = 0 \text{ for } t > t_0, \tag{22}$$

$$C = C_w \quad \text{at} \quad y = 0 \quad \text{for} \quad t > 0, \tag{23}$$

$$u \to 0, w \to 0, T \to T_\infty, \ C \to C_\infty \text{ as } y \to \infty \text{ for } t > 0. \tag{24}$$

For an optically thick fluid, in addition to emission, there is also self-absorption and usually the absorption coefficient is wave length dependent and large so we can adopt the Rosseland approximation for radiative heat flux vector q_r. Thus q_r is specified by

$$q_r = -\frac{4\sigma^*}{3k^*}\frac{\partial T^4}{\partial y}. \tag{25}$$

Assuming small temperature between the fluid temperature T and free stream temperature T_∞, T^4 is expanded mall in Taylor series concerning free stream temperature T_∞ to linearize equation (25), after overlooking second and higher order terms in $T - T_\infty$, it is assumed to the form be,

$$T^4 \cong 4T_\infty^3 T - 3T_\infty^4. \tag{26}$$

By using of Equations (25) and (26), Equation (17) reduces to,

$$\frac{\partial T}{\partial t} = \frac{k_1}{\rho C_p}\frac{\partial^2 T}{\partial y^2} + \frac{1}{\rho C_p}\frac{16\sigma^* T_\infty^3}{3k^*}\frac{\partial^2 T}{\partial y^2}. \tag{27}$$

We are introducing the dimensionless quantities,

$$y^* = \frac{y}{U_0 t_0}, u^* = \frac{u}{U_0}, w^* = \frac{w}{U_0}, t^* = \frac{t}{t_0}, \theta = \frac{T - T_\infty}{T_w - T_\infty}, \phi = \frac{(C - C_\infty)}{(C_w - C_\infty)}.$$

Making use of dimensionless quantities, Equations (15), (16), (18) and (27) are presented in the following forms,

$$(1+b)\frac{\partial u}{\partial t} + 2R^2 w = \frac{1}{1+\lambda_1}\left(1 + \lambda\frac{\partial}{\partial t}\right)\frac{\partial^2 u}{\partial y^2} - M^2(\alpha_1 u + \alpha_2 w) - \frac{u}{K(1+\lambda_1)} + \mathrm{Gr}\theta + \mathrm{Gc}\phi, \tag{28}$$

$$(1+b)\frac{\partial w}{\partial t} - 2R^2 u = \frac{1}{1+\lambda_1}\left(1 + \lambda\frac{\partial}{\partial t}\right)\frac{\partial^2 w}{\partial y^2} - M^2(\alpha_1 w - \alpha_2 u) - \frac{w}{K(1+\lambda_1)}, \tag{29}$$

$$\frac{\partial \theta}{\partial t} = \frac{(1+N)}{\mathrm{Pr}}\frac{\partial^2 \theta}{\partial y^2}, \tag{30}$$

$$\frac{\partial \phi}{\partial t} = \frac{1}{\mathrm{Sc}}\frac{\partial^2 \phi}{\partial y^2}, \tag{31}$$

where $M^2 = \frac{\sigma B_0^2 v}{\rho U_0^2}$ Hartmann number, $R^2 = \frac{v\Omega}{U_0^2}$ rotation parameter, $K = \frac{kU_0^2}{v\varphi}$ porosity parameter, $\lambda = \frac{\lambda_2 U_0^2}{\rho v^2}$ is the Jeffreys fluid parameter, $\mathrm{Gr} = \frac{g\beta v(\theta_w - \theta_\infty)}{U_0^3}$ thermal Grashof number, $\mathrm{Gc} = \frac{g\beta^* v(\phi_w - \phi_\infty)}{U_0^3}$

mass Grashof number, $\Pr = \frac{\nu\rho C_p}{k_1}$ Prandtl number $N = \frac{16\sigma^*\theta_\infty^3}{3k_1k^*}$ thermal-radiation parameter, $\mathrm{Sc} = \frac{\nu}{D}$ Schmidt number, $t_0 = \frac{\nu}{U_0^2}$.

Combining Equations (28) and (29), let $q = u + iw$,

$$(1+b)\frac{\partial q}{\partial t} = \frac{1}{1+\lambda_1}\left(1+\lambda\frac{\partial}{\partial t}\right)\frac{\partial^2 q}{\partial y^2} - \left(M^2(\alpha_1 - i\alpha_2) + \frac{1}{K(1+\lambda_1)} - 2iR^2\right)q + \mathrm{Gr}\theta + \mathrm{Gc}\phi \quad (32)$$

The relevant initial and boundary conditions are

$$q = 0,\ \theta = 0, \phi = 0 \quad \text{for} \quad y \geq 0 \text{ and } t \leq 0 \quad (33)$$

$$q = 1,\ \text{at } y = 0 \quad \text{for} \quad t > 0, \quad (34)$$

$$\theta = t,\ \text{at } y = 0 \quad \text{for} \quad 0 < t \leq 1, \quad (35)$$

$$\theta = 1,\ \text{at } y = 0 \quad \text{for} \quad t > 1, \quad (36)$$

$$\phi = 1,\ \text{at} \quad y = 0 \quad \text{for } t > 0, \quad (37)$$

$$q \to 0, \theta \to 0, \phi \to 0 \quad \text{as} \quad y \to \infty \text{ for } t > 0. \quad (38)$$

Equations (30), (31) and (32), after taking Laplace transform and using initial conditions (33) reduced to,

$$\frac{d^2\overline{q}}{dy^2} - \lambda_3\,\overline{q} = -\frac{(1+\lambda_1)\mathrm{Gr}}{(1+s\lambda)}\,\overline{\theta} - \frac{(1+\lambda_1)\mathrm{Gc}}{(1+s\lambda)}\,\overline{\phi}, \quad (39)$$

$$\frac{d^2\overline{\theta}}{dy^2} - sa\,\overline{\theta} = 0, \quad (40)$$

$$\frac{d^2\overline{\phi}}{dy^2} - s\mathrm{Sc}\,\overline{\phi} = 0, \quad (41)$$

where $a = \frac{\Pr}{1+N}$ and $b = \frac{\lambda}{K(1+\lambda_1)}$.

The boundary conditions (33)–(38) in the terms of transformed variables,

$$\overline{q} = \frac{1}{s}, \overline{\theta} = \frac{(1-e^{-s})}{s^2}, \overline{\phi} = \frac{1}{s} \quad \text{at } y = 0, \quad (42)$$

$$\overline{q} \to 0, \overline{\theta} \to 0, \overline{\phi} \to 0 \quad \text{as} \quad y \to \infty. \quad (43)$$

The transformed solutions of Equations (39), (40) and (41) with the boundary conditions (42) and (43) specified by,

$$\overline{q}(y,s) = \frac{1}{s}e^{-y\sqrt{\lambda_3}} + \frac{a_1(1-e^{-s})(1+\lambda s)}{s^2(s-\beta_1)}\{e^{-y\sqrt{\lambda_3}} - e^{-y\sqrt{sa}}\} + \frac{a_2(1+\lambda s)}{s(s+\beta_2)}\{e^{-y\sqrt{\lambda_3}} - e^{-y\sqrt{s\mathrm{Sc}}}\}, \quad (44)$$

$$\overline{\theta}(y,s) = \frac{(1-e^{-s})}{s^2}e^{-y\sqrt{sa}}, \quad (45)$$

$$\overline{\phi}(y,s) = \frac{1}{s^2}e^{-y\sqrt{s\mathrm{Sc}}}, \quad (46)$$

Taking the inverse Laplace transforms to Equations (44)–(46), therefore, it is acquired the exact solutions of the velocity, temperature and concentration distributions to be,

$$q(y,t) = q_0(y,t) + a_1\,(q_1(y,t) - H(t-1)\,q_1(y,t-1)) + a_2\,q_2(y,t), \tag{47}$$

$$\theta(y,t) = \theta_1(y,t) - H(t-1)\,\theta_1(y,t-1), \tag{48}$$

$$\phi(y,t) = \phi_1(y,t), \tag{49}$$

The expressions (47)–(49) represent the analytical solutions for fluid velocity, temperature and fluid concentration for natural convection MHD rotating flow of a viscous, incompressible, electrically conducting and optically thick heat radiating Jeffreys fluid past an impulsively moving vertical plate with ramped temperature taking Hall and ion slip effects into account and are valid when $a \neq 1$ and $\mathrm{Sc} \neq 1$.

2.1 | Limiting cases

Case 1 Substituting $a \neq 1$ and $\mathrm{Sc} = 1$ in Equation (47), (48) and (49), it is obtained that,

$$q(y,t) = q_0(y,t) + a_1\,(q_1(y,t) - H(t-1)\,q_1(y,t-1)) + a_3\,q_3(y,t) \tag{50}$$

$$\phi(y,t) = \phi_2(y,t) \tag{51}$$

In order to highlight the influence of ramped temperature distribution within the plate on the flow-field, it may be justified to compare such a flow with the one past an impulsively moving vertical plate with uniform temperature. Keeping in view the assumptions made in this paper, the solution for the fluid temperature and fluid velocity for the flow past an impulsively moving isothermal vertical plate is obtained and is presented in the following form

$$q(y,t) = q_4(y,t) \tag{52}$$

$$\theta(y,t) = \theta_2(y,t) \tag{53}$$

Case 2 Substituting $a = 1$ and $\mathrm{Sc} = 1$ in Equation (48) and (49), it is obtained that, the temperature and concentration are,

$$\theta(y,t) = \theta_4(y,t) \tag{54}$$

$$\phi(y,t) = \phi_2(y,t) \tag{55}$$

For isothermal plate,

$$\theta(y,t) = \theta_3(y,t) \tag{56}$$

Case 3 Substituting $a = 1$ and $\mathrm{Sc} \neq 1$ in the Equation (48) and (49), it is obtained that, the temperature is,

$$\theta(y,t) = \theta_4(y,t) \tag{57}$$

$$\phi(y,t) = \phi_1(y,t) \tag{58}$$

For isothermal plate,

$$\theta(y,t) = \theta_3(y,t) \tag{59}$$

The expressions for primary skin friction τ_x, secondary skin friction τ_z and Nusselt number Nu, these are computes of shear stress at the plate due to primary flow, shear stress at the plate due to secondary flow and rate of heat transfer at the plate respectively, are presented in the following form for the ramped temperature and isothermal plates.

$$\tau_w = \tau_x + i\tau_z = \frac{\mu}{1+\lambda_1}\left(1+\lambda\frac{\partial}{\partial t}\right)\left.\frac{\partial q}{\partial y}\right|_{y=0} \tag{60}$$

$$\mathrm{Nu} = -\left(\frac{\partial\theta}{\partial y}\right)_{y=0} \tag{61}$$

The Sherwood number Sh, is calculated of rate of mass transfer at the plate and is given by

$$\mathrm{Sh} = -\left(\frac{\partial\phi}{\partial y}\right)_{y=0} \tag{62}$$

where some expressions are mentioned in Appendix A.

$$\lambda_3 = \frac{1+\lambda_1}{1+\lambda s}\left((1+b)s + M^2(\alpha_1 - i\alpha_2) + \frac{1}{K(1+\lambda_1)} - 2iR^2\right),$$

$$M_1 = \frac{M^2(\alpha_1 - i\alpha_2) + (1/K(1+\lambda_1)) - 2iR^2}{1+b}$$

$$a_1 = \frac{\mathrm{Gr}}{a-1}, a_2 = \frac{\mathrm{Gc}}{\mathrm{Sc}-1}, a_3 = \frac{\mathrm{Gc}}{M_1}, a_4 = \frac{1+\lambda_1}{a-1}, a_5 = \frac{1+\lambda_1}{1-\mathrm{Sc}}, a_6 = a_1\left(\frac{1}{a_4} - \lambda\right).$$

This is remains significant to noted that for the validity of our results when the Jeffreys parameters λ_1 and $\lambda_2 \to 0$ we acquired the outcomes of Seth et al. [58] for viscous fluid, and if as well as Hartmann number $M \to 0$, and porosity parameter $K \to \infty$ with λ_1 and $\lambda_2 \to 0$ recovered the outcomes were found by Chandran et al. [59] equivalent to the incompressible viscous fluids.

3 | RESULTS AND DISCUSSION

It is considered the Hall and ion slip effects on the unsteady MHD rotating flow of a viscous, incompressible electrically conducting, and optically thick radiating Jeffreys fluid over an impulsively, moving vertical plate embedded in a saturated porous medium, when the temperature of the plate has a provisionally ramped profile. The exact solutions of the governing equations for the flow domain are attained by making use of the Laplace transform method. The flow is governed by the nondimensional parameters namely, Hartmann number M, porosity parameter K, rotation parameter R, Jeffreys fluid parameter λ, Hall parameter β_e, ion slip parameter β_i, Prandtl number Pr, Schmidt number Sc, thermal Grashof number Gr, mass Grashof number Gc, thermal radiation parameter N and time t.

Figures 2–18 represent the profiles of velocities, temperature for ramped wall temperature and isothermal plate, and concentration profiles respectively. The primary and secondary velocities execute a distinctive highest value near surface of the plate and then diminish properly on

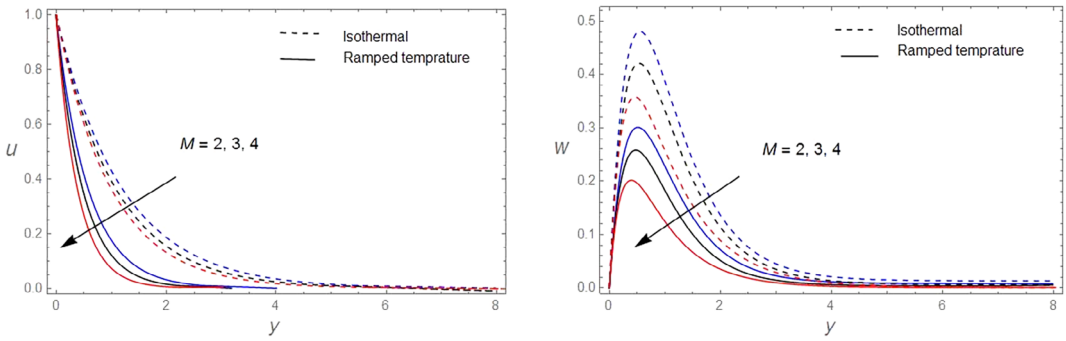

FIGURE 2 The velocity profiles for u and w against M with $R = 1$, $K = 0.5$, $\beta_e = 1$, $\beta_i = 0.2$, $\lambda = 1$, Pr = 0.71, $N = 2$, Sc = 0.22, Gr = 3, Gc = 5, $t = 0.2$ [Color figure can be viewed at wileyonlinelibrary.com]

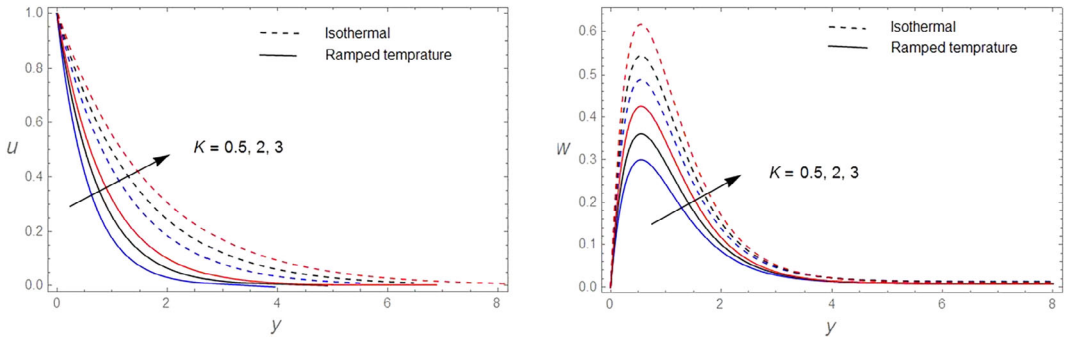

FIGURE 3 The velocity profiles for u and w against K with $M = 2$, $R = 1$, $\beta_e = 1$, $\beta_i = 0.2$, $\lambda = 1$, Pr = 0.71, $N = 2$, Sc = 0.22, Gr = 3, Gc = 5, $t = 0.2$ [Color figure can be viewed at wileyonlinelibrary.com]

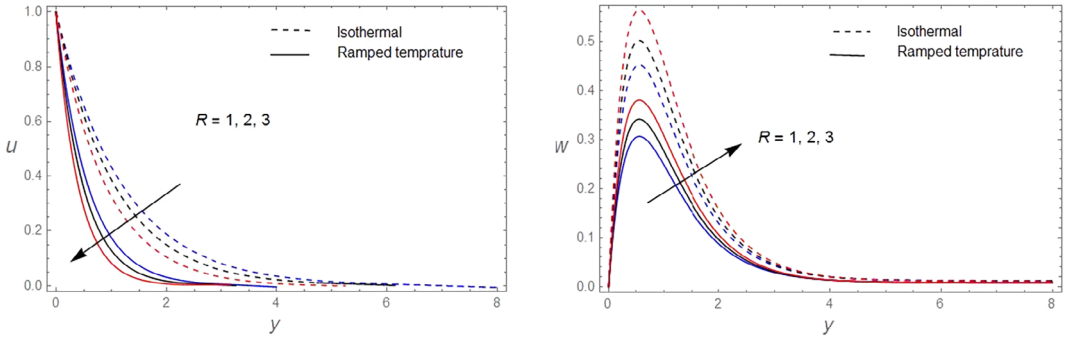

FIGURE 4 The velocity profiles for u and w against R with $M = 2$, $K = 0.5$, $\beta_e = 1$, $\beta_i = 0.2$, $\lambda = 1$, Pr = 0.71, $N = 2$, Sc = 0.22, Gr = 3, Gc = 5, $t = 0.2$ [Color figure can be viewed at wileyonlinelibrary.com]

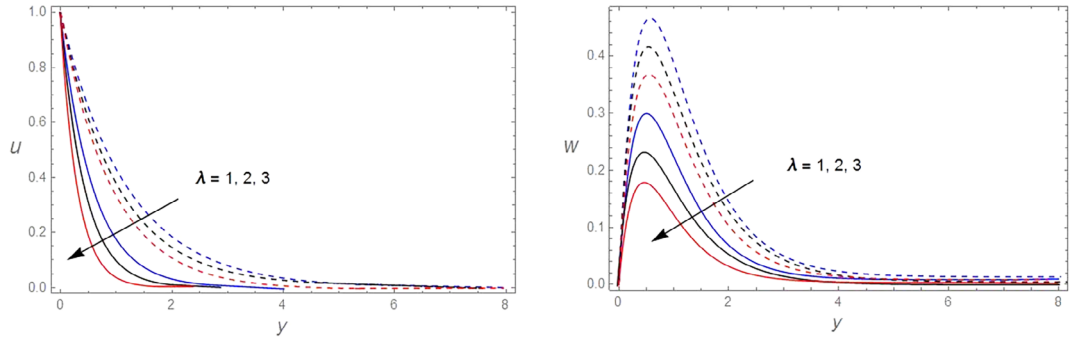

FIGURE 5 The velocity profiles for u and w against λ with $M = 2$, $R = 1$, $K = 0.5$, $\beta_e = 1$, $\beta_i = 0.2$, Pr = 0.71, $N = 2$, Sc = 0.22, Gr = 3, Gc = 5, $t = 0.2$ [Color figure can be viewed at wileyonlinelibrary.com]

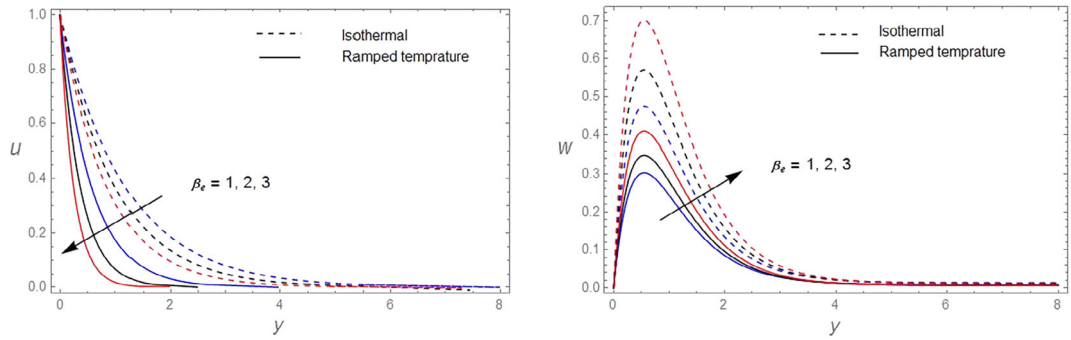

FIGURE 6 The velocity profiles for u and w against β_e with $M = 2$, $R = 1$, $K = 0.5$, $\lambda = 1$, $\beta_i = 0.2$, Pr = 0.71, $N = 2$, Sc = 0.22, Gr = 3, Gc = 5, $t = 0.2$ [Color figure can be viewed at wileyonlinelibrary.com]

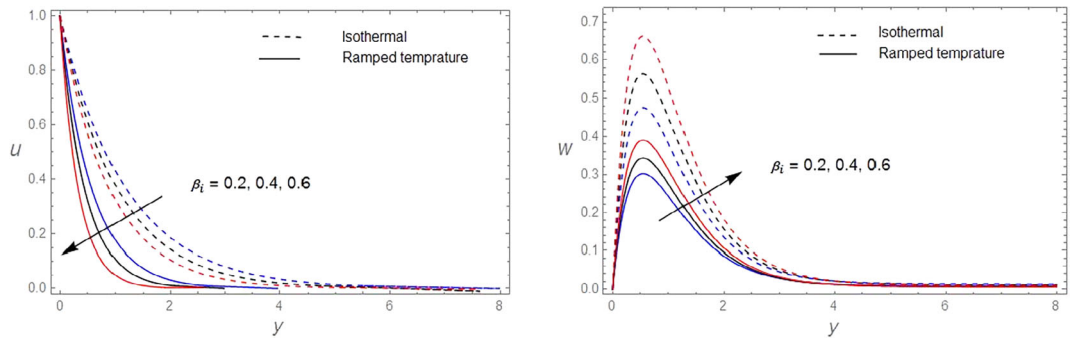

FIGURE 7 The velocity profiles for u and w against β_i with $M = 2$, $R = 1$, $K = 0.5$, $\lambda = 1$, $\beta_e = 1$, Pr = 0.71, $N = 2$, Sc = 0.22, Gr = 3, Gc = 5, $t = 0.2$ [Color figure can be viewed at wileyonlinelibrary.com]

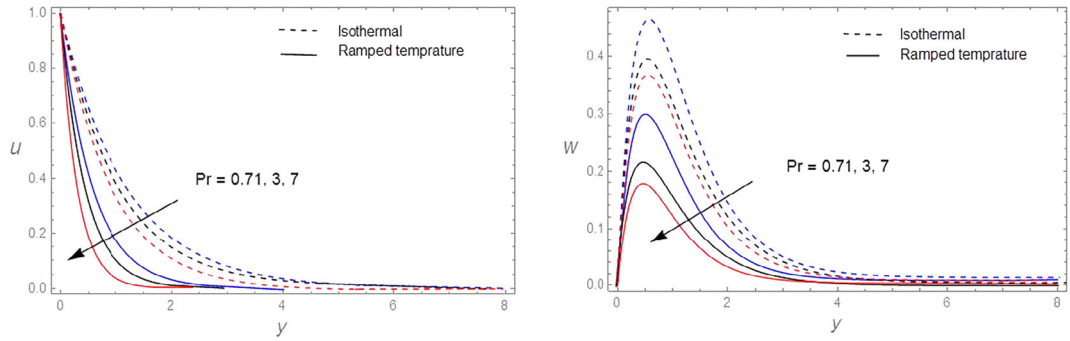

FIGURE 8 The velocity profiles for u and w against Pr with $M = 2$, $R = 1$, $K = 0.5$, $\beta_e = 1$, $\beta_i = 0.2$, $\lambda = 1$, $N = 2$, Sc = 0.22, Gr = 3, Gc = 5, $t = 0.2$ [Color figure can be viewed at wileyonlinelibrary.com]

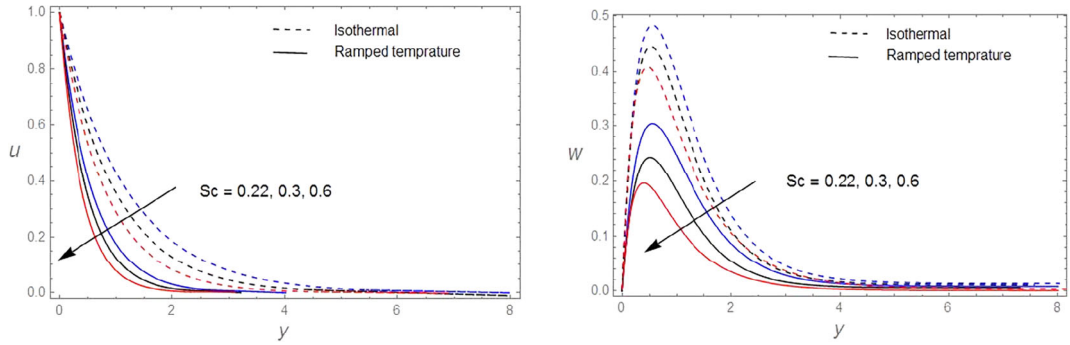

FIGURE 9 The velocity profiles for u and w against Sc with $M = 2$, $R = 1$, $K = 0.5$, $\beta_e = 1$, $\beta_i = 0.2$, $\lambda = 1$, Pr = 0.71, $N = 2$, Gr = 3, Gc = 5, $t = 0.2$ [Color figure can be viewed at wileyonlinelibrary.com]

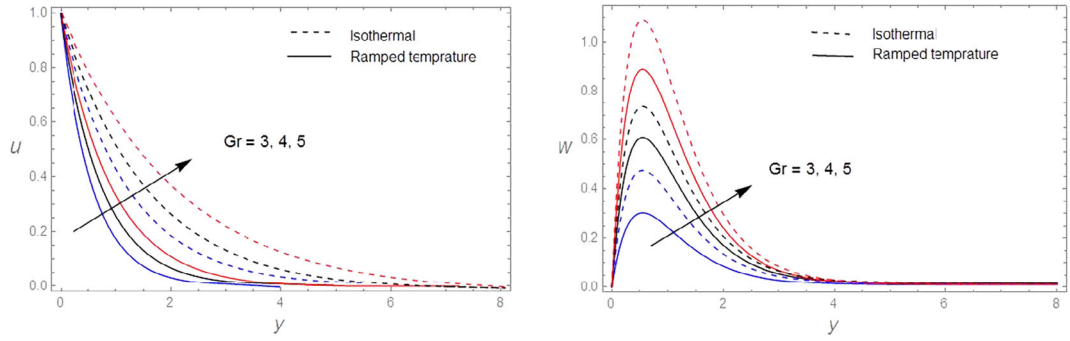

FIGURE 10 The velocity profiles for u and w against Gr with $M = 2$, $R = 1$, $K = 0.5$, $\beta_e = 1$, $\beta_i = 0.2$, $\lambda = 1$, Pr = 0.71, $N = 2$, Sc = 0.22, Gc = 5, $t = 0.2$ [Color figure can be viewed at wileyonlinelibrary.com]

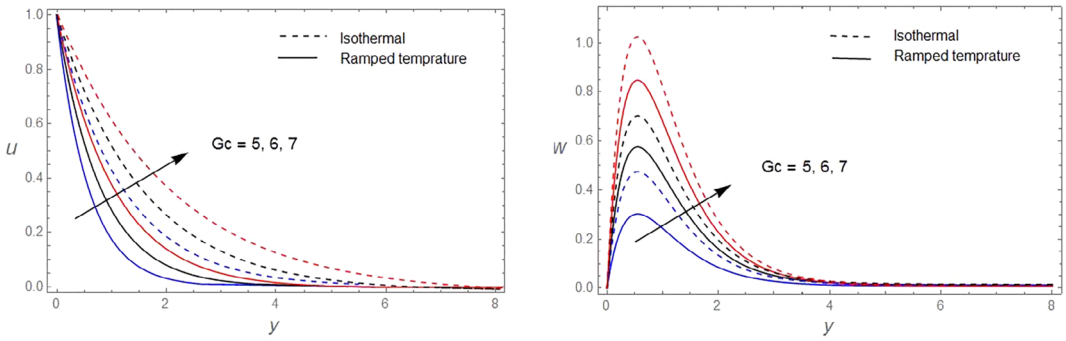

FIGURE 11 The velocity profiles for u and w against Gc with $M = 2$, $R = 1$, $K = 0.5$, $\beta_e = 1$, $\beta_i = 0.2$, $\lambda = 1$, Pr = 0.71, $N = 1$, Sc = 0.22, Gr = 3, $t = 0.2$ [Color figure can be viewed at wileyonlinelibrary.com]

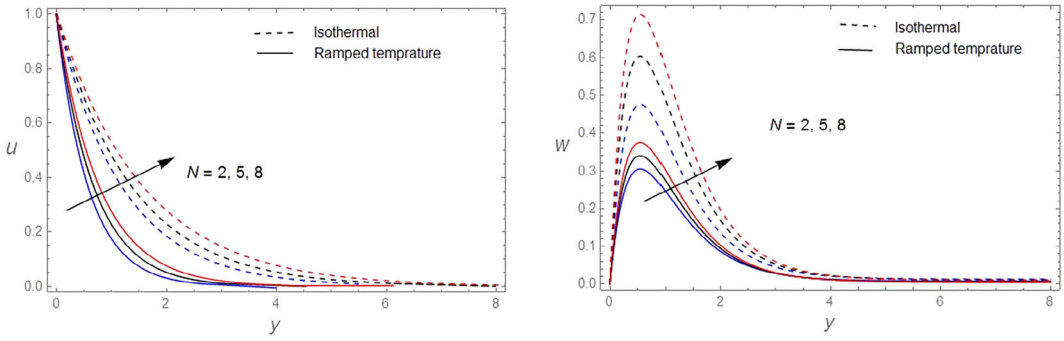

FIGURE 12 The velocity profiles for u and w against N with $M = 2$, $R = 1$, $K = 0.5$, $\beta_e = 1$, $\beta_i = 0.2$, $\lambda = 1$, Pr = 0.71, Sc = 0.22, Gr = 3, Gc = 5, $t = 0.2$ [Color figure can be viewed at wileyonlinelibrary.com]

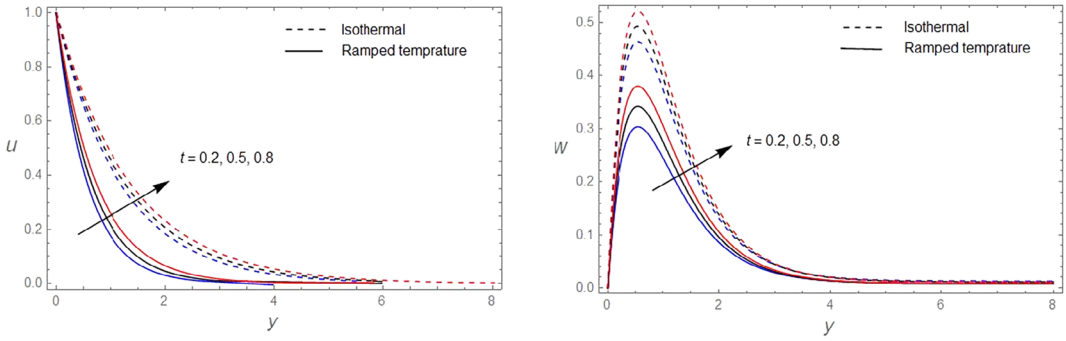

FIGURE 13 The velocity profiles for u and w against t with $M = 2$, $R = 1$, $K = 0.5$, $\beta_e = 1$, $\beta_i = 0.2$, $\lambda = 1$, Pr = 0.71, Sc = 0.22, Gr = 3, Gc = 5, $N = 2$ [Color figure can be viewed at wileyonlinelibrary.com]

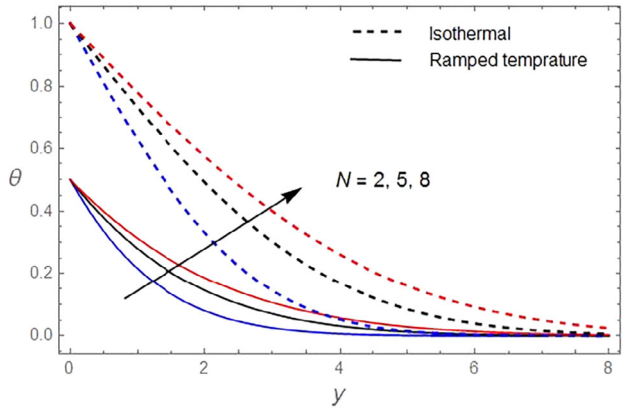

FIGURE 14 The temperature profiles against N with $\mathrm{Pr} = 0.71$, $t = 0.5$ [Color figure can be viewed at wileyonlinelibrary.com]

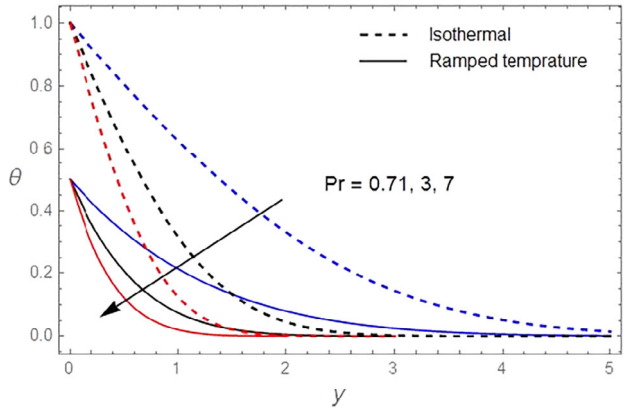

FIGURE 15 The temperature profiles against Pr with $N = 2$, $t = 0.5$ [Color figure can be viewed at wileyonlinelibrary.com]

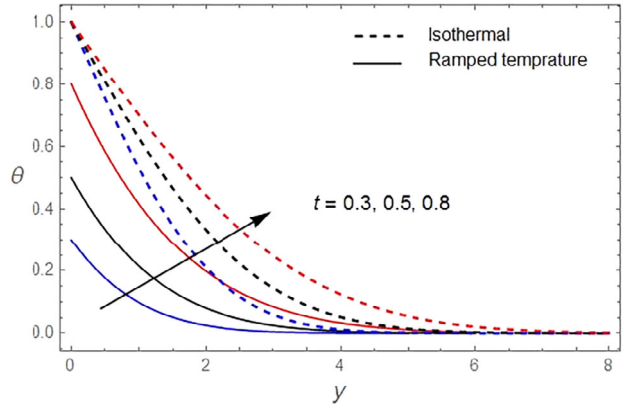

FIGURE 16 The temperature profiles against t with $N = 2$, $\mathrm{Pr} = 0.71$ [Color figure can be viewed at wileyonlinelibrary.com]

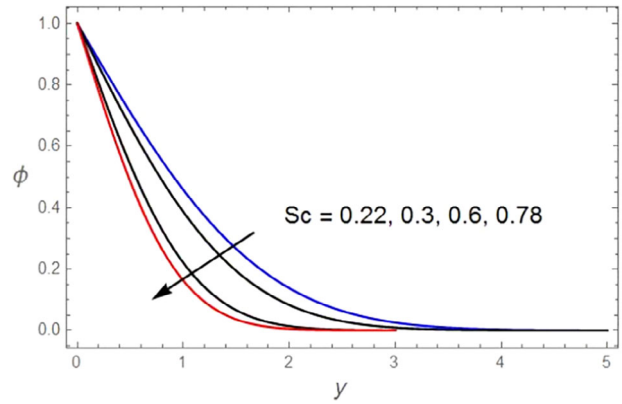

FIGURE 17 The concentration profiles against Sc with $t = 0.5$ [Color figure can be viewed at wileyonlinelibrary.com]

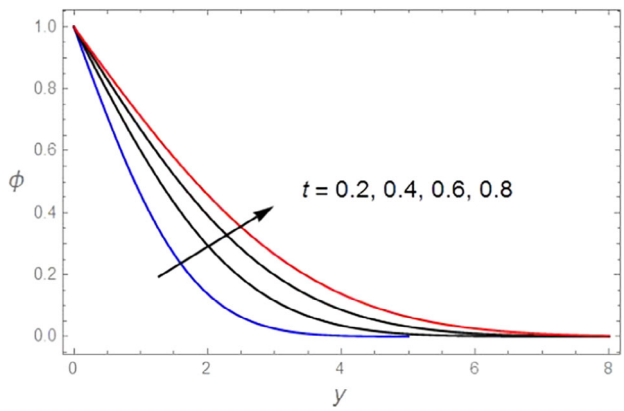

FIGURE 18 The concentration profiles against t with Sc = 0.22 [Color figure can be viewed at wileyonlinelibrary.com]

increasing boundary layer co-ordinate y to reach free stream conditions. It is also perceived that the primary and secondary velocities are slower down in the case of ramped temperature plate than that of isothermal plate. The skin friction, Nusselt number on both ramped temperature and isothermal plates, and Sherwood number are also computed and displayed in Tables 1–3.

When the magnetic field is large, then the Hall current will be developed in the flow field. Therefore, it is considered that the values of Hartmann number $0 < M \leq 4$ for Hall and ion slip effects; the values of the porosity parameter are $0 < K < 3$; rotation parameter $0 < R < 3$. Jeffreys fluid parameter $0 < \lambda < 3$; the values of the Hall parameter β_e are 1–3 ($\omega_e \tau_e \approx \mathrm{O}(1)$); the values of ion slip parameters β_i are 0 to less than 1 ($\omega_i \tau_i \ll 1$); It is also considered the values of Prandtl number Pr are 0.71, 3 and 7 for air, refrigerants and water respectively; It is picked the Schmidt number values as Sc = 0.22, 0.3, 0.6, 0.78 this corresponding to H_2, He, H_2O–vapor, and NH_3 respectively; thermal Grashof number $0 < \mathrm{Gr} < 10$, mass Grashof number $0 < \mathrm{Gm} < 10$, thermal radiation parameter $0 < N \leq 8$ [55, 60]. For computational purpose, it is fixed the quantities, the porosity $\varphi = 0.5$, the ratio of relaxation and retardation times $\lambda_1 = 0.5$, and considered as $M = 0.5$, $\beta_e = 1$, $\beta_i = 0.2$, $R = 1$, $K = 0.5$, $\lambda = 1$, Pr = 0.71, $N = 2$, Sc = 0.22, Gr = 3, Gc = 5, $t = 0.2$, while we illustrate the graphs on each parameter varied over the range.

Figure 2 displayed the effect of the Hartmann number on both primary and secondary velocity components u and w. This is evident that in each the ramped temperature and isothermal plate, the

TABLE 1 Skin friction (τ)

M	K	R	λ	β_e	β_i	Pr	Gr	Gc	N	Sc	t	Ramped $-\tau_x$	temperature τ_z	Isothermal $-\tau_x$	τ_z
0.5	0.5	1	1	1	0.2	0.71	3	5	2	0.22	0.2	2.86522	1.99985	2.16589	2.42544
1												3.15225	1.55244	1.87785	2.67025
1.5												3.42011	1.36522	1.71445	2.88547
	1											3.26558	2.33566	1.71662	1.86485
	1.5											3.65774	2.67588	1.25524	1.42415
		2										3.26658	2.15447	2.49969	2.86550
		3										3.66322	2.59855	2.88858	3.23324
			2									3.12100	2.30142	2.49996	2.89965
			3									3.53214	2.63552	2.96638	3.15526
				2								2.57485	2.25447	2.01145	2.77854
				3								2.33655	2.66589	1.62504	3.25501
					0.4							2.46255	2.23325	1.99999	2.68025
					0.6							2.23202	2.56525	1.53360	3.10025
						3						3.33255	1.83526	2.34255	2.23255
						7						3.67455	1.71145	2.62855	2.02256
							4					2.57885	2.34625	2.06658	2.67588
							5					2.02544	2.51774	1.89965	2.82145
								6				2.46988	2.16522	1.89899	2.86635
								7				2.15547	2.37996	1.53365	3.22214
									3			2.72011	2.00115	2.02144	2.46585
									4			2.61477	2.01552	1.90225	2.48854
										0.3		3.00144	1.81145	2.36556	2.23232
										0.6		3.15244	1.66636	2.53985	2.02565
											0.5	2.72104	2.14225	2.02114	2.96558
											0.8	2.52145	2.42885	1.96699	3.21044

TABLE 2 Nusselt number (Nu)

N	Pr	t	Ramped temperature	Isothermal plate
2	0.71	0.2	0.245493	0.613732
5			0.173590	0.433974
8			0.141735	0.354338
	3		0.504627	1.261570
	7		0.770830	1.927070
		0.5	0.388158	0.388158
		0.8	0.490985	0.306866

TABLE 3 Sherwood number (Sh)

Sc	t	Sh
0.22	0.2	−0.591727
0.3		−0.690988
0.6		−0.977205
0.78		−1.114190
	0.4	−0.418414
	0.6	−0.341634
	0.8	−0.295864

velocity components u and w are the proximal part of the reduction in the plate by the same nature throughout the fluid medium. Consequently, unexpected decrement in velocity is noted in the vicinity of the surface in the appearance of the magnetic field. Also, it has cleared that this incidence trim downs the velocity distribution by the side of all points. This reflects know that the introduction of a magnetic field, orthogonal towards the flow direction, a proclivity or attraction to produce the resistance recognized as Lorentz force, this shows a tendency to refuse to go along with the flow right the way through the fluid medium. As a result, it is obtained as the application of the magnetic field in the appearance of porous material, endorses a decelerating effect on the resultant velocity distribution as well as the thickness of the momentum boundary layer.

Figure 3 illustrated that, the effect of porosity parameter K on velocity components for both ramped temperature and isothermal plate. It is noticed that, the primary and secondary velocity components u and w are increasing with an increase in permeable parameter K throughout the fluid medium. It is evident that the larger values of K, enhances the resultant velocity and consequently enlarge the momentum boundary layer thickness. Lesser the permeability causes slighter the fluid speed is observed inside the flow medium occupied by the fluid.

Figure 4 demonstrated that, the impacts of rotation parameter R on the primary and secondary velocities for both ramped temperature and isothermal plate. This is perceived that, on both cases, the primary velocity component u diminishes on mounting in rotation parameter, whereas the secondary velocity component w augments on escalating in rotation in the fluid region away from the plate. This implies that, for both ramped temperature and isothermal plates, rotation tends to retard primary fluid velocity throughout the boundary layer region. Although rotation is known to induce secondary fluid velocity in the flow field by suppressing the primary fluid velocity, its accelerating effect is prevalent only in the region near to the plate whereas it has a reverse effect on secondary fluid velocity in the region away from the plate. This is due to the reason that Coriolis force is dominant in the region near to the axis of rotation.

This is apparent from Figure 5, both the primary and secondary velocity components u and w are decreasing with an increase in Jeffreys fluid parameter on either case of ramped wall temperature or isothermal plate and consequently the thickness of the boundary layer increases.

This is perceived from Figures 6 and 7 that, for both ramped wall temperature and isothermal plates, the primary velocity component u lessens on an increasing in Hall and ion-slip parameters β_e or β_i while the second velocity component w augments on an increasing in Hall and ion-slip parameters throughout the fluid medium. It is cleared that, as reinforcement in the Hall parameter and ion slip parameter, this results, enhanced the resultant velocity and the momentum boundary layer thickness throughout the fluid medium. The incorporation of Hall parameter reduces the effective conductance and consequently move downs the magnetic renitent fierceness. Also, the efficient conductivity increases as increase in the ion slip parameter, for that reason, the attenuation forces are decreasing; as a result, velocity intensifies.

Figures 8 and 9 exemplified the impact of thermal and mass diffusions for the primary and secondary velocities of fluid for the both ramped temperature and isothermal plates. We observed that in either case the velocities u or w diminishes on growing Pr and Sc. Hence thermal and mass diffusions are predisposed to accelerating primary and secondary velocities of fluid throughout the boundary layer region for two cases. This is happening due to the information that thermal and mass diffusions proposed a momentum to the thermal and solutal buoyancy forces accordingly.

Figures 10 and 11 depicted the special consequences of thermal and concentration buoyancy forces, both the fluid velocities u and w are escalating with an enlarge in thermal Grashof number Gr or mass Grashof number Gc. Thermal Grashof number defined the comparative forces of thermal buoyancy to viscosity, likewise, solutal Grashof number signifies the relative potency of concentration buoyancy

force to viscous force. Hence, Gr and Gc, boost up on an increase in the potencies of thermal and solutal buoyancy forces respectively. Here the free convection stream is satisfied due to thermal and solutal buoyancy forces; hence thermal and solutal forces have a propensity to speed up the primary and secondary velocities of fluid during the boundary layer region in either case. Hence the resultant velocity and thickness of the momentum boundary layer are increased with increase in either thermal Grashof number Gr or mass Grashof number Gc for both cases.

Figure 12 delineated the effects of thermal radiation parameter N on the primary and the secondary velocities of fluid of either case of ramped wall temperature or isothermal plate. For both cases, the primary velocity u and secondary velocity w raise on ever-increasing in thermal radiation parameter. This implies that, thermal radiation is expected to accelerate primary velocity and secondary velocity of fluid throughout the boundary layer region for both cases ramped wall temperature or isothermal plates.

Also, Figure 13 depict that the influence of time on the primary and secondary fluid velocities for both ramped temperature and isothermal plates. It is evident that, for both ramped temperature and isothermal plates, u and w increase on increasing t. This implies that resultant fluid velocity is getting accelerated with the progress of time throughout the boundary layer region for both ramped temperature and isothermal plates. Hence, thickness of momentum boundary layer is enhances with increase in time. Thus it may be concluded that thermal and concentration buoyancy forces, thermal and mass diffusions and thermal radiation tend to enlarge the thickness of modified Ekmann–Hartmann boundary layer for both ramped temperature and isothermal plates. The thickness of modified Ekmann–Hartmann boundary layer also increases with the progress of time.

The numerical values of fluid temperature θ, computed from the analytical solutions (48) and (52), are depicted graphically in Figures 14–16 for various values of thermal radiation parameter N, Prandtl number Pr and time t. It is evident from Figure 14 that fluid temperature increases on increasing thermal radiation parameter N for both ramped temperature and isothermal plates. Thus thermal radiation tends to enhance fluid temperature throughout the boundary layer region for both ramped temperature and isothermal plates. This is consistent with the fact that thermal radiation provides an additional means to diffuse energy because thermal radiation parameter N and, therefore, an increase in N implies a decrease in Rosseland mean absorption coefficient for fixed values of T_∞ and k_1. Figures 15 and 16 reveal that fluid temperature decreases on increasing Prandtl number Pr whereas it increases on increasing t for both ramped temperature and isothermal plates. This implies that, for both ramped temperature and isothermal plates, thermal diffusion tends to enhance fluid temperature and there is an enhancement in fluid temperature with the progress of time throughout the boundary layer region.

The species concentration ϕ is computed from the exact solution (49), is presented graphically in Figures 17 and 18 for various values of Schmidt number Sc and time t. It is evident that, the species concentration decreases on increasing Sc whereas it increases on increasing t. This implies that mass diffusion tends to enhance species concentration and there is an enhancement in species concentration with the progress of time throughout the boundary layer region.

The numerical values of primary and secondary skin frictions τ_x and τ_z, computed from analytical expression (54), are presented in tabular form in Table 1 for various values of pertinent parameters. It is evident that, the primary and secondary skin-friction components τ_x increases and τ_z decreases with increasing Hartmann number for the ramped temperature and reversal behavior is attained for the isothermal plate. Although for the cases of ramped temperature and isothermal plate, the components τ_x declines and τ_z enhances with an increase in thermal radiation parameter N, thermal Grashof number Gr, mass Grashof number Gc, time t, Hall and ion slip parameters β_e and β_i, whereas τ_x enlarges and τ_z diminishes on raise in Prandtl number or Schmidt number Sc. Also the components τ_x and τ_z are enhanced on an increase in rotation parameter R or Jeffreys liquid parameter λ. Moreover both

TABLE 4 Results comparison for the primary velocity component (u) (Gc = 5, Pr = 0.71, Sc = 0.22, $N = 2$, $z = 0.5$, $t = 0.2$)

M	K	R	Gr	Previous results Seth et al. [60]	Present results $\lambda = \beta_e = \beta_i = 0$
0.5	0.5	1	3	0.225885	0.227481
1				0.214514	0.214526
1.5				0.203526	0.203363
	1.0			0.241444	0.241256
	1.5			0.259541	0.259665
		2		0.250415	0.250363
		3		0.289996	0.289885
			4	0.240255	0.240263
			5	0.261254	0.261152

stress components are mounting for the ramped temperature and lessen for an isothermal plate with an increase in porosity parameter K (Table 1). From Table 2, It is noticed that, the Nusselt number declines with an increase in thermal radiation parameter N, also it is enlarged on an increase in Prandtl number Pr at both cases of ramped temperature and isothermal plate. It is evident from fact that, for a given time, Nusselt number Nu is proportional to $\sqrt{a}$ in both the cases, that is, Nusselt number Nu increases on increasing Prandtl number Pr while it decreases on increasing thermal radiation parameter N. Since Pr is a measure of the relative strength of viscosity to thermal diffusivity of the fluid, Pr decreases on increasing thermal diffusivity of the fluid. This implies that thermal diffusion and thermal radiation tend to reduce rate of heat transfer at both the ramped temperature and isothermal plates. Also Nu increases for ramped temperature plate whereas it decreases for isothermal plate on increasing time t. This implies that rate of heat transfer at ramped temperature plate is enhanced whereas it is reduced at isothermal plate with the progress of time. It reveals that the Sherwood number is increasing with an increase in Schmidt number and there is refuse on rise in time (Table 3). Since Schmidt number Sc is a measure of the relative strength of viscosity to mass diffusivity of the fluid, Sc decreases on increasing mass diffusivity of the fluid. Thus we conclude that mass diffusion tends to reduce rate of mass transfer at the plate and there is reduction in rate of mass transfer at the plate with the progress of time.

4 | CODE VALIDATION

The exactitude of numerical code is simulated for propriety, by MATHEMATICA 10.4 software through the Laplace transformation mechanism. Using MATHEMTICA code, it is obtained the primary velocity distributions are shown in Table 4 for quite a few values of pertinent parameters namely Hartmann number, porosity parameter, rotation parameter and thermal Grashof number. Again, by using same code for the previous work [60], the same results are obtained nearly described above and are shown in Table 4 respectively for numerous values of pertinent parameters. The rigorously identical results are distinguished for both the research problems. Thus, the sensitivity of coding achieved accuracy.

5 | CONCLUSIONS

It is investigated theoretically that, Hall and ion slip effects on the unsteady MHD flow of a viscous, incompressible electrically conducting, and optically thick radiating Jeffreys fluid over an impulsively,

moving vertical plate embedded in a saturated porous medium, when the temperature of the plate has a provisionally ramped profile. The significant observations are made for both ramped wall temperature and isothermal plate. The rotation parameter has a tendency to increase secondary velocity, and to decelerate primary velocity throughout the boundary layer region. The resultant velocity enhances with an increase in Hall and ion slip parameters. Reversal behavior is observed with an increase in magnetic field parameter, Jeffreys fluid parameter and Prandtl number. Thermal and concentration buoyancy forces and thermal radiation tend to accelerate the resultant velocity throughout the boundary layer region. The temperature reduces with an increase Prandtl number and reverse effect is observed with an increase in thermal radiation parameter. Mass diffusion tends to enhance to species concentration. The rotation and Jeffreys fluid parameters tend to enhance both stress components. Nusselt number enables to lessen with growing in thermal radiation parameter and is magnified on escalating in time. The Sherwood number is improved with increasing in Schmidt number at the plate and it is refused on increasing in time.

NOMENCLATURE

u, w	fluid velocities in x and z directions (m/s)
t	time (s)
t_0	characteristic time (s)
T	dimensional temperature of the fluid (K)
C	dimensional species concentration of the fluid (kg/m^3)
T_w	the uniform temperature of the fluid at the plate (K)
C_w	the uniform concentration of the fluid at the plate (kg/m^3)
T_∞	the temperature of the fluid far away from the plate (K)
C_∞	the concentration of the fluid far away from the plate (kg/m^3)
g	acceleration due to gravity (m/s^2)
k	permeability of porous medium (m^2)
k^*	Rossland mean absorption co-efficient
C_p	specific heat at constant pressure (J/kg K)
q_r	radiative heat flux (W/m^2)
D	coefficient of mass diffusivity (m^2/s)
k_1	thermal conductivity of the fluid (W/m/K)
q	complex velocity (m/s)
$\mathbf{B}$	the magnetic field vector (A/m)
$\mathbf{E}$	the electric field (c)
$\mathbf{V}$	velocity vector (m/s)
$\mathbf{J}$	the current density vector (A/m^2)
B_0	applied magnetic field (A/m)
U_0	uniform velocity of the plate (m/s)
M	Hartmann number
R	rotation parameter
K	porosity parameter
Gr	thermal Grashof number
Gc	mass Grashof number
Pr	Prandtl number
N	thermal radiation parameter
Sc	the Schmidt number

Nu	Nusselt number
Sh	Sherwood number
$H(t-1)$	unit step function
$erfc(x)$	complementary error function

GREEK SYMBOLS

θ	nondimensional temperature of the fluid
ϕ	nondimensional species concentration of the fluid
β	volumetric coefficient of thermal expansion
β^*	volumetric coefficient of expansion for species concentration
ω_e	the cyclotron frequency (e/mB)
τ_e	the electron collision time (s)
φ	porosity
λ	Jeffreys fluid parameter
β_e	Hall parameter
β_i	ion slip parameter
μ_e	magnetic permeability (H/m)
σ^*	Stefan–Boltzmann constant
ν	kinematic viscosity of the fluid (m^2/s)
σ	electrical conductivity (s/m)
ρ	fluid density (kg/m^3)
Ω	angular velocity (s^{-1})

SUBSCRIPTS

e	electron
r	radiation

ORCID

M. Veera Krishna https://orcid.org/0000-0002-6580-1592

REFERENCES

[1] I. S. Awaludin, P. D. Weidman, and A. Ishak, *Stability analysis of stagnation-point flow over a stretching/shrinking sheet*, AIP Adv. 6 (2016), 045308. https://doi.org/10.1063/1.4947130.
[2] A. Bejan and K. R. Khair, *Heat and mass transfer by natural convection in a porous medium*, Int. J. Heat Mass Transf. 28 (1985), 909–918.
[3] A. J. Chamkha, H. S. Takhar, and V. M. Soundalgekar, *Radiation effects on free convection flow past a semi-infinite vertical plate with mass transfer*, Chem. Eng. J. 84 (2001), 335–342.
[4] E. R. Eckert and R. M. Drake, *Analysis of heat and mass transfer*, McGraw Hill, New York, 1972.
[5] P. Ganesan and G. Palani, *Natural convection effects on impulsively started inclined plate with heat and mass transfer*, Heat Mass Transf. 39 (2003), 277–283.
[6] B. Gebhart et al., *Buoyancy induced flow and transport*, Hemisphere, New York, 1998.
[7] J. Y. Jang and W. J. Chang, *Buoyancy-induced inclined boundary layer flow in a porous medium resulting from combined heat and mass buoyancy effects*, Int. Commun. Heat Mass Transf. 15 (1988), 17–30.
[8] F. C. Lai and F. A. Kulacki, *Non-Darcy mixed convection along a vertical wall in a saturated porous medium*, J. Heat Transf. 113 (1991), 252–255.
[9] A. Nakayama and M. A. Hossain, *An integral treatment for combined heat and mass transfer by natural convection in a porous medium*, Int. J. Heat Mass Transf. 38 (1995), 761–765.
[10] D. A. Nield and A. Bejan, *Convection in porous media*, 3rd ed., Springer, New York, 2006.

[11] I. Pop and D. B. Ingham, *Convective heat transfer: Mathematical and computational modelling of viscous fluids and porous media*, Pergamon, Oxford, 2001.
[12] A. A. Raptis, *Free convection and mass transfer effects on the oscillatory flow past an infinite moving vertical isothermal plate with constant suction and heat sources*, Astrophys. Space Sci. 86 (1982), 43–53.
[13] D. Ruchika, P. Rana, and L. Kumar, *Multiple solutions of MHD boundary layer flow and heat transfer behaviour of nanofluids induced by a power-law stretching/shrinking permeable sheet with viscous dissipation*, Powder Tech. 273 (2015), 62–70. https://doi.org/10.1016/j.powtec.2014.12.035.
[14] M. V. Krishna and A. J. Chamkha, *Hall and ion slip effects on MHD rotating flow of elastico-viscous fluid through porous medium*, Int. Commun. Heat Mass Transf. 113 (2020), 104494. https://doi.org/10.1016/j.icheatmasstransfer.2020.104494.
[15] M. V. Krishna, C. S. Sravanthi, and R. S. R. Gorla, *Hall and ion slip effects on MHD rotating flow of ciliary propulsion of microscopic organism through porous media*, Int. Commun. Heat Mass Transf. 112 (2020), 104500. https://doi.org/10.1016/j.icheatmasstransfer.2020.104500.
[16] M. Abd El-Aziz, *Dual solutions in hydromagnetic stagnation point flow and heat transfer towards a stretching/shrinking sheet with non-uniform heat source/sink and variable surface heat flux*, J. Egypt. Math. Soc. 24 (2016), 479–486. https://doi.org/10.1016/j.joems.2015.09.004.
[17] A. Shahzad et al., *Unsteady axisymmetric flow and heat transfer over time-dependent radially stretching sheet*, Alexandria Eng. J 56 (2017), 35–41. https://doi.org/10.1016/j.aej.2016.08.030.
[18] M. Turkyilmazoglu, *Flow of a micropolar fluid due to a porous stretching sheet and heat transfer*, Int. J. Non-Linear Mech. 83 (2016), 59–64. https://doi.org/10.1016/j.ijnonlinmec.2016.04.004.
[19] S. Baag et al., *Entropy generation analysis for viscoelastic MHD flow over a stretching sheet embedded in a porous medium*, Ain Shams Eng. J. 8 (2016), 623–632. https://doi.org/10.1016/j.asej.2015.10.017.
[20] J. Ahmed et al., *MHD axisymmetric flow of power law fluid over an unsteady stretching sheet with convective boundary conditions*, Results Phys. 6 (2016), 973–981. https://doi.org/10.1016/j.rinp.2016.11.013.
[21] N. F. Fauzi, S. Ahmad, and I. Pop, *Stagnation point flow and heat transfer over a nonlinear shrinking sheet with slip effects*, Alexandria Eng. J. 54 (2015), 929–934. https://doi.org/10.1016/j.aej.2015.08.004.
[22] A. K. Hakeem, V. N. Ganesh, and B. Ganga, *Magnetic field effect on second order slip flow of nanofluid over a stretching/shrinking sheet with thermal radiation effect*, J. Magnetism Magnetic Mater. 381 (2015), 243–257. https://doi.org/10.1016/j.jmmm.2014.12.010.
[23] K. Bhattacharyya and I. Pop, *MHD boundary layer flow due to an exponentially shrinking sheet*, MHD 47(4) (2011), 337–344.
[24] K. Bhattacharyya, *Effects of radiation and heat source/sink on unsteady MHD boundary layer flow and heat transfer over a shrinking sheet with suction/injection*, Frontiers Chem. Sci. Eng. 5 (2011), 376–384. https://doi.org/10.1007/s11705-011-1121-0.
[25] K. Bhattacharyya, *Effects of heat source/sink on MHD flow and heat transfer over a shrinking sheet with mass suction*, Chem. Eng. Res. Bullit. 15 (2011), 12–17. https://doi.org/10.3329/cerb.v15i1.6524.
[26] M. Imtiaz, T. Hayat, and A. Alsaedi, *MHD convective flow of Jeffreys fluid due to a curved stretching surface with homogeneous–heterogeneous reactions*, PLoS ONE 11 (2016), e0161641. https://doi.org/10.1371/journal.pone.0161641.
[27] N. Sandeep and C. Sulochana, *Momentum and heat transfer behaviour of Jeffreys, Maxwell and Oldroyd-B nanofluids past a stretching surface with non-uniform heat source/sink*, Ain Shams Eng. J. 9 (2016), 517–524. https://doi.org/10.1016/j.asej.2016.02.008.
[28] K. Ahmad, Z. Hanouf, and A. Ishak, *Mixed convection Jeffreys fluid flow over an exponentially stretching sheet with magnetohydrodynamic effect*, AIP Adv. 6 (2016), 035024. https://doi.org/10.1063/1.4945401.
[29] T. Hayat et al., *MHD stagnation point flow of Jeffreys fluid by a radially stretching surface with viscous dissipation and Joule heating*, J. Hydrology Hydromech. 63 (2015), 311–317. https://doi.org/10.1515/johh-2015-0038.
[30] D. Kalidas, N. Acharya, and P. K. Kundu, *Radiative flow of MHD Jeffreys fluid past a stretching sheet with surface slip and melting heat transfer*, Alexandria Eng. J. 54 (2015), 815–821. https://doi.org/10.1016/j.aej.2015.06.008.
[31] M. V. Krishna, G. S. Reddy, and A. J. Chamkha, *Hall effects on unsteady MHD oscillatory free convective flow of second grade fluid through porous medium between two vertical plates*, Phys. Flu. 30 (2018), 023106. https://doi.org/10.1063/1.5010863.
[32] M. V. Krishna and A. J. Chamkha, *Hall effects on unsteady MHD flow of second grade fluid through porous medium with ramped wall temperature and ramped surface concentration*, Phys. Flu. 30 (2018), 053101. http://doi.org/10.1063/1.5025542.
[33] M. V. Krishna and A. J. Chamkha, *Hall and ion slip effects on unsteady MHD convective rotating flow of nanofluids—Application in biomedical engineering*, J. Egypt. Math. Soc. 28(1) (2020), 1–14. https://doi.org/10.1186/s42787-019-0065-2.
[34] M. V. Krishna, N. A. Ahamad, and A. J. Chamkha, *Hall and ion slip effects on unsteady MHD free convective rotating flow through a saturated porous medium over an exponential accelerated plate*, Alexandria Eng. J. 59 (2020), 565–577. https://doi.org/10.1016/j.aej.2020.01.043.

[35] M. V. Krishna, K. Bharathi, and A. J. Chamkha, *Hall effects on MHD peristaltic flow of Jeffrey fluid through porous medium in a vertical stratum*, Interf. Phenom. Heat Transf. 6(3) (2019), 253–268. https://doi.org/10.1615/InterfacPhenomHeatTransfer.2019030215.
[36] M. Hashemi-Tilehnoee et al., *Magneto-fluid dynamic and second law analysis in a hot porous cavity filled by nanofluid and nano-encapsulated phase change material suspension with different layout of cooling channels*, J. Energy Storage 31 (2020), 101720. https://doi.org/10.1016/j.est.2020.101720.
[37] M. S. Sadeghi et al., *Analysis of hydrothermal characteristics of magnetic Al_2O_3–H_2O nanofluid within a novel wavy enclosure during natural convection process considering internal heat generation*, Math. Methods Appl. Sci. 43 (2020), 1–13. https://doi.org/10.1002/mma.6520.
[38] S. Mondal et al., *A theoretical nanofluid analysis exhibiting hydromagnetics characteristics employing CVFEM*, J Braz. Soc. Mech. Sci. Eng. 42 (2020), 19. https://doi.org/10.1007/s40430-019-2103-2.
[39] A. S. Dogonchi et al., *Simulation of Fe_3O_4–H_2O nanoliquid in a triangular enclosure subjected to Cattaneo–Christov theory of heat conduction*, Int. J. Numer. Methods Heat Fluid Flow 29 (2019), 4430–4444. https://doi.org/10.1108/HFF-01-2019-0031.
[40] M. Hashemi-Tilehnoee et al., *Entropy generation in concentric annuli of 400 kV gas-insulated transmission line*, Thermal Sci. Eng. Progress 19 (2020), 100614. https://doi.org/10.1016/j.tsep.2020.100614.
[41] J. K. Singh, G. S. Seth, and S. Vishwanath, *Impacts of the periodic wall conditions to the hydromagnetic convective flow of viscoelastic fluid through a vertical channel with Hall current and induced magnetic field*, Heat Transf. 49 (2020), 1–24. https://doi.org/10.1002/htj.21957.
[42] J. K. Singh, G. S. Seth, and S. Vishwanath, *Hall and ion-slip effects on MHD free convective flow of a viscoelastic fluid through porous regime in an inclined channel with moving magnetic field*, Kragujevac J. Sci. 42 (2020), 5–18. https://doi.org/10.5937/KgJSci2042005K.
[43] J. K. Singh et al., *Steady MHD mixed convection flow of a viscoelastic fluid over a magnetized convectively heated vertical surface with Hall current and induced magnetic field effects*, Heat Transf. 49 (2020), 1–24. https://doi.org/10.1002/htj.21831.
[44] J. K. Singh et al., *Hydromagnetic free convective flow of Walters'-B fluid over a vertical surface with time varying surface conditions*, World J. Eng. 17 (2020), 295–307. https://doi.org/10.1108/WJE-06-2019-0163.
[45] J. K. Singh, N. Joshi, and P. Rohidas, *Unsteady MHD natural convective flow of a rotating Walters'-B fluid over an oscillating plate with fluctuating wall temperature and concentration*, J. Mech. 34 (2018), 529–532. https://doi.org/10.1017/jmech.2017.25.
[46] J. K. Singh, G. S. Seth, and S. G. Begum, *Unsteady MHD natural convection flow of a rotating visco-elastic fluid over an infinite vertical porous plate due to oscillating free-stream*, Multidisci. Model. Mater. Struc. 14 (2018), 236–260. https://doi.org/10.1108/MMMS-06-2017-0054.
[47] J. K. Singh, S. G. Begum, and G. S. Seth, *Influence of Hall current and wall conductivity on hydromagnetic mixed convective flow in a rotating Darcian channel*, Phys. Fluids 30 (2018), 113602. https://doi.org/10.1063/1.5054654.
[48] G. S. Seth and J. K. Singh, *Mixed convection hydromagnetic flow in a rotating channel with Hall and wall conduction effects*, Appl. Math. Model. 40 (2016), 2783–2803. https://doi.org/10.1016/j.apm.2015.10.015.
[49] A. I. Alsabery et al., *Entropy generation and natural convection flow of hybrid nanofluids in a partially divided wavy cavity including solid blocks*, Energies 13 (2020), 2942. https://doi.org/10.3390/en13112942.
[50] M. Ghalambaz et al., *Study of thermal and hydrodynamic characteristics of water-nano-encapsulated phase change particles suspension in an annulus of a porous eccentric horizontal cylinder*, Int. J. Heat Mass Transf. 156 (2020), 119792. https://doi.org/10.1016/j.ijheatmasstransfer.2020.119792.
[51] S. M. H. Zadeh et al., *Thermo-hydrodynamic and entropy generation analysis of a dilute aqueous suspension enhanced with nano-encapsulated phase change material*, Int. J. Mech. Sci. 178 (2020), 105609. https://doi.org/10.1016/j.ijmecsci.2020.105609.
[52] S. A. M. Mehryan et al., *Natural convection flow of a suspension containing nano-encapsulated phase change particles in an eccentric annulus*, J. Energy Storage 28 (2020), 101236. https://doi.org/10.1016/j.est.2020.101236.
[53] M. Ghalambaz et al., *Analysis of melting behavior of PCMs in a cavity subject to a non-uniform magnetic field using a moving grid technique*, Applied Math. Model. 77 (2020), 1936–1953. https://doi.org/10.1016/j.apm.2019.09.015.
[54] S. A. M. Mehryan et al., *Melting heat transfer of power-law non-Newtonian phase change nano-enhanced n-octadecane-mesoporous silica ($MPSiO_2$)*, Int. J. Heat Mass Transf. 151 (2020), 119385. https://doi.org/10.1016/j.ijheatmasstransfer.2020.119385.
[55] M. V. Krishna, *Hall and ion slip impacts on unsteady MHD free convection rotating flow of Jefferys fluid with ramped wall temperature*, Int. Commun. Heat Mass Transf. 119 (2020), 104927. https://doi.org/10.1016/j.icheatmasstransfer.2020.104927.
[56] K. Maqbool, A. B. Mann, and M. H. Tiwana, *Unsteady MHD convective flow of a Jeffreys fluid embedded in a porous medium with ramped wall velocity and temperature*, Alexandria Eng. J. 57 (2018), 1071–1078. https://doi.org/10.1016/j.aej.2017.02.012.
[57] G. Sutton and A. Sherman, *Engineering magnetohydrodynamics*, McGraw Hill, New York, 1965.

[58] G. S. Seth, M. S. Ansari, and R. Nandkeolyar, *MHD natural convection flow with radiative heat transfer past an impulsively moving plate with ramped wall temperature*, Heat Mass Transf. 47 (2011), 551–561.
[59] P. Chandran, N. C. Sacheti, and A. K. Singh, *Natural convection near a vertical plate with ramped wall temperature*, Heat Mass Transf. 41 (2005), 459–464.
[60] G. S. Seth, S. Sarkar, and S. M. Hussian, *Effects of Hall current, radiation and rotation on natural convection heat and mass transfer flow past a moving vertical plate*, Ain Shams Eng. J. 5 (2014), 489–503. https://doi.org/10.1016/j.asej.2013.09.014.

How to cite this article: Krishna MV, Chamkha AJ. Hall and ion slip effects on magnetohydrodynamic convective rotating flow of Jeffreys fluid over an impulsively moving vertical plate embedded in a saturated porous medium with Ramped wall temperature. *Numer Methods Partial Differential Eq.* 2020;1–28. https://doi.org/10.1002/num.22670

APPENDIX A.

$$\phi_1(y,t) = erfc\left(\frac{y}{2}\sqrt{\frac{\mathrm{Sc}}{t}}\right),\ \phi_2(y,t) = erfc\left(\frac{y}{2\sqrt{t}}\right)$$

$$\theta_1(y,t) = \left(t + \frac{ay^2}{2}\right)\ erfc\left(\frac{y}{2}\sqrt{\frac{a}{t}}\right) - \sqrt{\frac{at}{\pi}}\, y\, e^{-\frac{ay^2}{4t}}$$

$$\theta_2(y,t) = erfc\left(\frac{y}{2}\sqrt{\frac{a}{t}}\right),\ \theta_3(y,t) = erfc\left(\frac{y}{2\sqrt{t}}\right)$$

$$\theta_4(y,t) = \left(t + \frac{y^2}{2}\right)\ erfc\left(\frac{y}{2}\sqrt{\frac{1}{t}}\right) - \sqrt{\frac{t}{\pi}}\, y\, e^{-\frac{y^2}{4t}}$$

$$q_0(y,t) = \frac{1}{2}\left(e^{y\sqrt{M_1}} erfc\left(\frac{y}{2\sqrt{t}} + \sqrt{M_1 t}\right) + e^{-y\sqrt{\lambda}} erfc\left(\frac{y}{2\sqrt{t}} - \sqrt{M_1 t}\right)\right)$$

$$\begin{aligned} q_1(y,t) = \frac{1}{2}\Bigg\{ & \frac{e^{a_4 t}}{a_4^2}\left(e^{y\sqrt{(\lambda+a_4)}} erfc\left(\frac{y}{2\sqrt{t}} + \sqrt{(\lambda+a_4)t}\right) + e^{-y\sqrt{(\lambda+a_4)}} erfc\left(\frac{y}{2\sqrt{t}} - \sqrt{(\lambda+a_4)t}\right)\right. \\ & \left. -e^{y\sqrt{(aa_4)}} erfc\left(\frac{y}{2}\sqrt{\frac{a}{t}} + \sqrt{a_4 t}\right) - e^{-y\sqrt{(aa_4)}} erfc\left(\frac{y}{2}\sqrt{\frac{a}{t}} - \sqrt{a_4 t}\right)\right) \\ & - \frac{1}{\beta_1}\Bigg\{\left(t + \frac{1}{a_4} + \frac{y}{2\sqrt{\lambda}}\right) e^{y\sqrt{\lambda}} erfc\left(\frac{y}{2\sqrt{t}} + \sqrt{\lambda t}\right) \\ & + \left(t + \frac{1}{a_4} - \frac{y}{2\sqrt{\lambda}}\right) e^{-y\sqrt{\lambda}} erfc\left(\frac{y}{2\sqrt{t}} - \sqrt{\lambda t}\right) \\ & -2\left(t + \frac{1}{a_4} + \frac{ay^2}{2}\right) erfc\left(\frac{y}{2}\sqrt{\frac{a}{t}}\right) + 2\sqrt{\frac{at}{\pi}}\, y e^{-\frac{ay^2}{4t}}\Bigg\} \end{aligned}$$

$$+\lambda^2 e^{\left(\frac{-1}{\lambda}\right)t}\left(e^{y\sqrt{y-\frac{1}{\lambda}}}\,erfc\left(\frac{y}{2\sqrt{t}}+\sqrt{\left(M_1-\frac{1}{\lambda}\right)t}\right)+e^{-y\sqrt{y-\frac{1}{\lambda}}}\,erfc\left(\frac{y}{2\sqrt{t}}-\sqrt{\left(M_1-\frac{1}{\lambda}\right)t}\right)\right.$$
$$\left.-e^{y\sqrt{\frac{-a}{\lambda}}}\,erfc\left(\frac{y}{2}\sqrt{\frac{a}{t}}+\sqrt{\left(\frac{-1}{\lambda}\right)t}\right)-e^{-y\sqrt{\frac{-a}{\lambda}}}\,erfc\left(\frac{y}{2}\sqrt{\frac{a}{t}}-\sqrt{\left(\frac{-1}{\lambda}\right)t}\right)\right)\Bigg\}$$

$$q_2(y,t)=\frac{1}{2a_5(1-a_5\lambda)}$$
$$\left(e^{y\sqrt{M_1}}\,erfc\left(\frac{y}{2\sqrt{t}}+\sqrt{M_1 t}\right)+e^{-y\sqrt{M_1}}\,erfc\left(\frac{y}{2\sqrt{t}}-\sqrt{M_1 t}\right)-2erfc\left(\frac{y}{2}\sqrt{\frac{\mathrm{Sc}}{t}}\right)\right.$$
$$-e^{-a_5 t}\left\{e^{y\sqrt{\frac{M_1-a_5}{1-a_5\lambda}}}\,erfc\left(\frac{y}{2\sqrt{t}}+\sqrt{\left(\frac{M_1-a_5}{1-a_5\lambda}\right)t}\right)+e^{-y\sqrt{\frac{M_1-a_5}{1-a_5\lambda}}}\,erfc\left(\frac{y}{2\sqrt{t}}-\sqrt{\left(\frac{M_1-a_5}{1-a_5\lambda}\right)t}\right)\right.$$
$$-e^{iy\sqrt{\mathrm{Sc}\;a_5}}erfc\left(\frac{y}{2}\sqrt{\frac{\mathrm{Sc}}{t}}+i\sqrt{a_5 t}\right)-e^{-iy\sqrt{\mathrm{Sc}\;a_5}}erfc\left(\frac{y}{2}\sqrt{\frac{\mathrm{Sc}}{t}}-i\sqrt{a_5 t}\right)$$
$$\left.-\;e^{iy\sqrt{\mathrm{Sc}\;(-1/\lambda)}}erfc\left(\frac{y}{2}\sqrt{\frac{\mathrm{Sc}}{t}}+i\sqrt{(-1/\lambda)t}\right)-e^{-iy\sqrt{\mathrm{Sc}\;(-1/\lambda)}}erfc\left(\frac{y}{2}\sqrt{\frac{\mathrm{Sc}}{t}}-i\sqrt{(-1/\lambda)t}\right)\right\}\Bigg)$$
$$q_3(y,t)=\frac{1}{2}\left\{\left(t+\frac{y}{2\sqrt{M_1}}\right)e^{y\sqrt{M_1}}erfc\left(\frac{y}{2\sqrt{t}}+\sqrt{M_1 t}\right)\right.$$
$$\left.+\left(t-\frac{y}{2\sqrt{M_1}}\right)e^{-y\sqrt{\lambda}}erfc\left(\frac{y}{2\sqrt{t}}-\sqrt{M_1 t}\right)-2erfc\left(\frac{y}{2\sqrt{t}}\right)\right\}$$

$$q_4(y,t)=\frac{(1-a_6)}{2}\left[e^{y\sqrt{M_1}}erfc\left(\frac{y}{2\sqrt{t}}+\sqrt{M_1 t}\right)+e^{-y\sqrt{M_1}}erfc\left(\frac{y}{2\sqrt{t}}-\sqrt{M_1 t}\right)\right]$$
$$+\frac{a_1}{a_4}\frac{e^{a_4 t}}{2}\left(\left\{e^{y\sqrt{(\lambda+a_4)}}erfc\left(\frac{y}{2\sqrt{t}}+\sqrt{(\lambda+a_4)t}\right)+e^{-y\sqrt{(\lambda+a_4)}}erfc\left(\frac{y}{2\sqrt{t}}-\sqrt{(\lambda+a_4)t}\right)\right\}\right.$$
$$\left.-\left\{e^{y\sqrt{aa_4}}erfc\left(\frac{y}{2}\sqrt{\frac{a}{t}}+\sqrt{a_4 t}\right)+e^{-y\sqrt{aa_4}}erfc\left(\frac{y}{2}\sqrt{\frac{a}{t}}-\sqrt{a_4 t}\right)\right\}\right)$$
$$-a_1\lambda\frac{e^{\left(\frac{-1}{\lambda}\right)t}}{2}\left(\left\{e^{y\sqrt{M_1-\frac{1}{\lambda}}}\,erfc\left(\frac{y}{2\sqrt{t}}+\sqrt{\left(M_1-\frac{1}{\lambda}\right)t}\right)+e^{-y\sqrt{M_1-\frac{1}{\lambda}}}erfc\left(\frac{y}{2\sqrt{t}}-\sqrt{(M_1+a_4)t}\right)\right\}\right.$$
$$\left.-\left\{e^{y\sqrt{\frac{-a}{\lambda}}}erfc\left(\frac{y}{2}\sqrt{\frac{a}{t}}+\sqrt{(-1/\lambda)t}\right)+e^{-y\sqrt{\frac{-a}{\lambda}}}erfc\left(\frac{y}{2}\sqrt{\frac{a}{t}}-\sqrt{(-1/\lambda)t}\right)\right\}\right)$$
$$+a_6\,erfc\left(\frac{y}{2}\sqrt{\frac{a}{t}}\right)+a_2\,q_2(y,t)$$

For the ramped temperature,

$$\tau_w=\sqrt{M_1}(erfc(\sqrt{M_1 t})-1)-(1/\sqrt{\pi t})e^{-M_1 t}+a_1(q_5(0,\mathrm{t})-H(\mathrm{t}-1)\,q_5(0,t-1))]+a_2 q_6(0,t)$$

$$Nu=2\sqrt{a/\pi}\;[\sqrt{t}-\sqrt{(t-1)}H(t-1)]$$

For the isothermal plate

$$\tau_w = (1-a_6)\sqrt{M_1}(erfc(\sqrt{M_1 t})-1) - (1/\sqrt{\pi t})e^{-M_1 t}$$
$$-(a_1/a_4)e^{a_4 t}\{\sqrt{(M_1+a_4)}(erfc(\sqrt{(M_1+a_4)t})-1) - \sqrt{aa_4}(erfc(\sqrt{aa_4 t})-1)\}$$
$$+\lambda e^{\left(\frac{-1}{\lambda}\right)t}\left\{\sqrt{M_1-\frac{1}{\lambda}}\left(erfc\sqrt{\left(M_1-\frac{1}{\lambda}\right)t}-1\right) - \sqrt{\left(\frac{-a}{\lambda}\right)}\left(erfc\sqrt{a\left(\frac{-1}{\lambda}\right)t}-1\right)\right\}$$
$$-a_2 q_6(0,t)$$

$$Nu = \sqrt{\frac{a}{\pi t}}$$

$$q_5(0,t) = \frac{e^{a_4 t}}{a_4^2}[\sqrt{(M_1+a_4)}\{erfc(\sqrt{(M_1+a_4)t})-1\} - \sqrt{aa_4}\{erfc(\sqrt{a_4 t})-1\}]$$
$$-\lambda^2 e^{-\left(\frac{1}{\lambda}\right)t}\left[\sqrt{\left(M_1-\frac{1}{\lambda}\right)}\left\{erfc\left(\sqrt{\left(M_1-\frac{1}{\lambda}\right)t}\right)-1\right\}\right.$$
$$\left.-\sqrt{a\left(\frac{-1}{\lambda}\right)}\left\{erfc\left(\sqrt{\left(\frac{-1}{\lambda}\right)t}\right)-1\right\}\right]$$
$$+\frac{\lambda}{a_4}\left[\left\{\left(t+\frac{1}{a_4}-\lambda\right)\sqrt{M_1}+\frac{1}{2\sqrt{M_1}}\right\}\{erfc(\sqrt{M_1 t})-1\} - \sqrt{\frac{t}{\pi}}(e^{-M_1 t}-\sqrt{a})\right]$$

$$q_6(0,t) = -\frac{\lambda}{a_5}\left(\sqrt{M_1}\{erfc(\sqrt{M_1 t})-1\} + \frac{1}{\sqrt{\pi t}}(2\sqrt{\mathrm{Sc}}-1) - \right.$$
$$-e^{-a_5 t}\{\sqrt{M_1-a_5}(erc\sqrt{(M_1-a_5)t}-1) - i\sqrt{\mathrm{Sc}\,a_5}(erfc\sqrt{ia_5 t}-1)\}$$
$$\left.-e^{-\left(\frac{1}{\lambda}\right)t}\left\{\sqrt{M_1+\frac{1}{\lambda}}\left(erf\sqrt{\left(M_1+\frac{1}{\lambda}\right)t}-1\right) - i\sqrt{\frac{\mathrm{Sc}}{\lambda}}\left(erfc\sqrt{i\left(\frac{-1}{\lambda}\right)t}-1\right)\right\}\right)$$

$$Sh = -\sqrt{\frac{\mathrm{Sc}}{\pi t}}$$